Consumption of atmospheric methane by the Qinghai–Tibetan Plateau alpine steppe ecosystem

Hanbo Yun[1, 2, 3], Qingbai Wu[1*], Qianlai Zhuang[3*], Anping Chen[4*] Tong Yu[3], Zhou Lyu[3], Yuzhong Yang[1], Huijun Jin[1], Guojun Liu[1], Yang Qu[3], Licheng Liu[3]

1. State Key Laboratory of Frozen Soil Engineering, Northwest Institute of Eco–Environment and Resources, Chinese Academy of Sciences, Lanzhou, Gansu 730000, China

2. Key Laboratory for Land Surface Process and Climate Change in Cold and Arid Regions, Chinese Academy of Sciences, Lanzhou, 730000, China

3. Department of Earth, Atmospheric, and Planetary Sciences, Purdue University, West Lafayette, Indiana 47907, USA

4. Department of Forestry and Natural Resources, Purdue University, West Lafayette, Indiana 47907, USA

*Authors for correspondence: qbwu@lzb.ac.cn [Q. W.]，qzhuang@purdue.edu[Q.Z], apchen1111@gmail.com [A.C.]

A manuscript for *The Cryosphere*

May 30, 2018

Abstract

The Methane (CH_4) cycle on the Qinghai–Tibetan Plateau (QTP), the world's largest high–elevation permafrost region, is sensitive to climate change and subsequent freezing and thawing dynamics. Yet, its magnitudes, patterns, and environmental controls are still poorly understood. Here, we report results from five continuous year–round CH_4 observations from a typical alpine steppe ecosystem in the QTP permafrost region. Our results suggest that the QTP permafrost region was a CH_4 sink of -0.86 ± 0.23 g CH_4–C m^{-2} yr^{-1} over 2012 – 2016, a rate higher than that of many other permafrost areas, such as the Arctic tundra in northern Greenland, Alaska, and western Siberia. Soil temperature and soil water content were dominant factors controlling CH_4 fluxes, however, their correlations changed with soil depths, due to freezing and thawing dynamics. This region was a net CH_4 sink in autumn, but a net source in spring, despite both seasons experiencing similar top soil thawing and freezing dynamics. The opposite CH_4 source/sink function in spring versus in autumn was likely caused by the respective seasons specialized freezing and thawing processes, which modified the vertical distribution of soil layers that are highly mixed in autumn, but not in spring. Furthermore, the traditional definition of four seasons failed to capture the pattern of the annual CH_4 cycle. We developed a new seasonal division method based on soil temperature, bacterial activity, and permafrost active layer thickness, which significantly improved the modelling of the annual CH_4 cycle. Collectively, our findings highlight the critical role of fine–scale climate freezing and thawing dynamics in driving permafrost CH_4 dynamics, which needs to be better monitored and modelled in Earth system models.

1. Introduction

Since 2007, the global atmospheric methane concentration [CH$_4$] continues to rise, after remaining stable between the 1990s and 2006 (Rigby et al., 2008; IPCC, 2013; Patra and Kort, 2016). Understanding mechanisms for this recent increase requires improved knowledge on CH$_4$ sources and sinks for regional and global CH$_4$ budgets (Kirschke et al., 2013; Zona et al., 2016). However, estimates on global CH$_4$ emissions and consumptions are still highly uncertain (Spahni et al., 2011; Kirschke, 2013). In particular, the bottom–up approach, which estimates CH$_4$ budgets using ground observations and inventory, overestimated the global CH$_4$ budget by 6～20 times, compared to the atmospherically constrained top–down approach (Zhu et al., 2004; Lau et al., 2015). This discrepancy is partly due to limited monitoring data and to our poor understanding of important factors regulating the production and consumption of CH$_4$ (Whalen and Reeburgh, 1990; Dengel et al., 2013; Bohn et al., 2015).

The Qinghai–Tibetan Plateau (QTP) is the world's largest high–elevation permafrost region of 1.23×10^6 km^2 (Wang et al., 2000). The QTP is currently experiencing a rapid change in climate, which affects freezing and thawing processes. The change in the freezing and thawing dynamics profoundly impacts methanotrophy and methanogenesis, which consequently impacts net CH$_4$ fluxes (Mastepanov *et al.*, 2013; Lau et al., 2015). However, due to the scarcity of year-round monitoring data at high temporal resolution, we still know little about the size, seasonal pattern, and underlying controls of climate and permafrost freezing and thawing, and the resulting effects on CH$_4$ exchanges in the QTP permafrost region (Cao et al., 2008; Wei et al., 2015a; Song et al., 2015;). This knowledge gap also hampers our capacity to predict and understand QTP permafrost CH$_4$ cycles under current and projected future climates.

66   Here, we report results from a 5–year continuous *in situ* monitoring of CH_4 dynamics

67   with an eddy covariance (EC) technique at the Beilu'he Research Station, which is a

68   representative site for QTP permafrost heartland. The site was covered by alpine steppe

69   vegetation from January 1st, 2012 to December 31st, 2016. The primary aims of this investigation

70   are to understand (1) the long-term annual and seasonal variation of the methane budget for a

71   typical alpine permafrost site in the QTP, and (2) the environmental factors controlling these CH_4

72   variations and possible underlying mechanisms. In addition, while the consumption and

73   production of ecosystem methane are known through microbial activities, conventional

74   investigations on seasonal methane fluxes usually used climate or vegetation defined "seasons".

75   Therefore, a third research goal of this current study is to investigate if the classical vegetation

76   productivity-based definition of growing season will be useful for defining the methane flux

77   seasonality.

78   There are three advantages of our data acquisition system. First, the EC system recorded

79   the data of CH_4 fluxes, climate, and soil properties every half hour. As the QTP permafrost is

80   characterized by a rapidly changing climate and a rapidly changing soil freezing and thawing

81   dynamics, even over a time period as short as one day, different aerobic or anaerobic soil

82   environments that favor different types of CH_4 bacteria may change (Rivkina et al., 2004; Lau et

83   al., 2015). Thus, high–resolution *in situ* monitoring data enables us to quantify CH_4 exchange

84   patterns from diel to annual time–scales and investigate their major environmental drivers.

85   Second, our field investigation spanned five full calendar years, including both plant growing

86   and non–growing seasons. Observations of the plant non–growing season, which accounts for

87   two-thirds of a year, are very rare in current literature (Song et al., 2015). Third, the EC system

88   we used overcame some technical problems caused by the often used static chambers, including

89 limited representation of local site heterogeneity and additional heating of the soil surface

90 (Chang et al., 2014; Wei et al., 2015b).

91 **2. Methods**

92 **2.1 Site Description**

93 The research site, Beilu'he permafrost research station (34° 09' 006" N, 92° 02' 080" E),

94 is located in the alpine steppe continuous permafrost area of the northern QTP, about 320

95 kilometers southwest of Golmud, Qinghai Province (Figure 1). At an elevation of 4765 meters,

96 the air is thin with only 0.6 standard atmospheric pressure. According to *in situ* observations, the

97 site receives solar radiation of about 213.10 W m^{-2}. The non–growing season is long and cold,

98 with 225 days per year having an annual air temperature of -18 °C on average from 2012 to

99 2016. The site's growing season is short and cool, with 140 days per year from 2012 to 2016,

100 and a mean annual air temperature of 4.6 °C. According to the site drilling exploration, the

101 permafrost depth can extend to $50 - 70$ m below ground, and the thickness of the active layer

102 (ALT) is about $2.2 - 4.8$ m (Wu et al., 2010a). The soil is composed of Quaternary fine sand or

103 silt (Table 1), overlying on Triassic mudstone or weathered marl. Dominant plant species

104 include: *Carex moorcroftii* Falc. *ex* Boott, *Kobresia tibetica* Maxim, *Androsace*

105 *tanggulashanensis*, and *Rhodiola tibetica.* Vegetation coverage is approximately 33.5% and the

106 average plant height is 15 cm.

107 **2.2 Eddy Covariance observations**

108 We have continuously monitored CH_4, carbon dioxide (CO_2), water (H_2O), and heat flux

109 using a standard eddy covariance system tower 3 meters above the ground. CH_4 flux was measured

110 with an open-path CH_4 analyzer system (Figure 1d; LI–7700, LI–COR Inc., Lincoln, NE, USA).

111   The precision is 5 ppb, with RMS noise at 10 Hz and 2000 ppb. The instrument was placed on site

112   on August 8th, 2011, and then connected to a three–dimensional sonic anemometer (heat and water

113   flux; CSAT3, Campbell Scientific, and Logan, UT, USA; the precision is 0.1 °C with an accuracy

114   within 1% of reading for half–hour measurements) and an open–path infrared gas analyzer (CO_2

115   flux; LI–7500A, LI–COR Inc., Lincoln, NE, USA; the precision is $0.01 \mu mol \ m^{-2} \ s^{-1}$ with an

116   accuracy within 1% of reading for half–hour measurements, zero drift per °C is typically $\pm$ 0.1

117   ppm) on January 1st, 2012, when the system worked steadily. Monitoring data was recorded and

118   stored at 10 Hz using a data logger (LI–7550, LI–COR Inc., Lincoln, NE, USA).

119   The operation, calibrations, and maintenance of the EC system followed standard

120   procedures. To reduce the LI–7500A surface heating/cooling influence on CO_2 and H_2O molar

121   densities in tough environments, each year "summer style" was used in Li–7500A, in which

122   surface temperature setting is 5 °C during May 1st to September 30th. "Winter style" was used from

123   October 1st to the next year April 30th in Li–7500A, in which surface temperature setting is -5 °C.

124   Calibrations of CO_2, water vapor, and dew point generator measurements for LI–7500A analyzers

125   were performed regularly by the China Land–Atmosphere Coordinated Observation System

126   (CLAROS). Up–and–down mirrors of LI–COR 7700 were cleaned regularly every 30 days to

127   make sure the signal strength was stronger than 80. All of these instruments were powered by

128   solar–panel and battery.

129   **2.3 Micrometeorological and Soil Measurements**

130   A wide range of meteorological variables were measured by a standard automatic

131   meteorological tower 3 meters above the ground and 5 meters north of the eddy covariance

132   tower. Net radiation (Rn) and albedo were measured with a four–component radiometer (Rn;

133   CNR–1, Kipp and Zonen, the Netherlands). Air temperature (T_{air}), air relative humidity, and

atmospheric pressure were measured with a temperature and humidity sensor (HMP45C, Vaisala Inc., Helsinki, Finland) in the meteorological tower. A rain gauge (TE525MM, Texas Electronics Inc., Dallas, TX, USA) was used to measure precipitation. Wind speed and direction were observed using a propeller anemometer placed on the top of the meteorological tower.

We also measured soil heat fluxes, soil temperature and soil relative water content (SWC). In August 2010, we installed sensors for soil environment and surface energy exchange monitoring 10 m apart from the eddy covariance tower. Two self–calibrating soil heat flux (SHF) sensors (HFP01) were placed 5 cm and 15 cm below the ground. A group pF–Meter sensor (GEO–Precision, Germany) was embedded in the soil under the meteorological tower to measure soil temperature (T_{soil}) at 0 cm, 5 cm, 10 cm, 15 cm, 20 cm, 30 cm, 40 cm, 50 cm, 70 cm, 80 cm, 100 cm, 150 cm, 160 cm, and 200 cm depth. The pF meter sensors also measured SWC at 10 cm, 20 cm, 40 cm, 80 cm, and 160cm depth.

All of above environmental parameters were synchronously monitored with eddy covariance, and the data was recorded every 30 minutes by CR3000 (Data logger, Campbell Data Taker Ltd, Salt Lake City, UT, USA). The air temperature sensors, the humidity sensors, and the pF meter sensors were calibrated in the State Key Laboratory of Frozen Soil Engineering at the Chinese Academy of Sciences in order to ensure the measurement accuracy was within $\pm$ 0.05 °C and $\pm$ 5%, respectively.

We also sampled soil profiles for soil physical and chemical measurements with one 1 m $\times$ 1 m $\times$ 2 m pit 10 m apart from the eddy covariance tower in August 2010. Five profile samples were taken from the pit at depths 0 − 20 cm, 20 − 50 cm, 50 − 120 cm, 120 − 160 cm, and 160 − 200 cm. Sampling at each depth was repeated five times and the samples of the same

156   depths were then well mixed. After that, the mixed soil sample of each depth was stored in

157   aluminum boxes and carefully sealed to prevent gas exchanges with air. The clod method was

158   used to investigate the field wet bulk density (weight of soil per unit volume; Cate and Nelson,

159   1971). The soil moisture content was calculated gravimetrically by the ratio of the mass of water

160   present to the oven–dry (60 °C for 24 hour) weight of the soil sample. The soil organic carbon

161   (SOC) content of the air–dried soil samples was analyzed using the wet combustion method,

162   Walkley–Black modified acid dichromate digestion, $FeSO_4$ titration, and an automatic titrator.

163   Total nitrogen (TN) and pH were measured using standard soil test procedures from the Chinese

164   Ecosystem Research Network.

165   To understand the potential effect of soil thawing and freezing dynamics on CH_4 fluxes,

166   we also reconstructed and verified semi-monthly data of soil active layer thickness (ALT).

167   Following Muller's original definition, ALT is the maximum thaw depth in the late autumn using

168   a linear interpolation of T_{soil} profiles between two neighboring points above and below the 0 °C

169   isotherm (Muller, 1947). We used records of the soil thawing thickness measured with a self–

170   made geological probe to verify the ALT data semi–monthly. More information about the

171   measurement procedure was previously described by Wu and Zhang (2010a).

172   **2.4 Microbial Activity**

173   To understand how soil microbial activity may have impacted the CH_4 fluxes, we sampled

174   100 g soils for soil microbial activity measurements. These soils were obtained using a soil

175   sample drill device (Ø=0.03 m), with depths of $0 - 25$ cm taken every 5 days within 100 m of the

176   eddy covariance tower. The sampled soil was fully mixed and divided into two equal parts. Each

177   part was then stored in sterilized aluminum boxes and then placed in liquid nitrogen, before

178   sending to the lab for microbe RNA extraction. We then used a real-time PCR method to

8

179   genetically test methanotrophic / archaeal methanogens, and the procedure was repeated three

180   times for each sample. By setting the maximum methanotrophic / archaeal methanogens gene

181   expression cyclic number as 1, we calculated the variety coefficient of methanotrophic and

182   archaeal methanogens gene expressions (ΔI and ΔII, respectively; %) with equation (1):

183    $$\Delta_i = {x_I}/{X_{Max}}$$ …   (1)

184   Δ_i is for the ith methanotrophic/archaeal methanogens gene expression; x_i is the

185   methanotrophic / archaeal methanogen gene expression cyclic number of the ith time; X_{Max} is the

186   maximum methanotrophic / archaeal methanogen gene expression cyclic number of the soil

187   group from 2012 to 2016.

188   **2.5 EC Data Processing and Data Filtering**

189   Data collected from January 1st, 2012 to December 31st, 2016 was used in this study. Before

190   processing, we removed data that was recorded at the time of precipitation events or with LI–7700

191   signal strength under 85. We first processed the raw data in EddyPro (version 6.2.0, LI–COR,

192   Lincoln, NE, USA). We adopted standardized procedures recommended in Lee et al. (2006) to

193   process half–hourly flux raw measurements to ensure their quality.

194   1) Data was processed through statistical analysis in EddyPro including: spike removal

195   (accepted spikes < 5% and replaced spikes with linear interpolation), amplitude resolution (range

196   of variation: 7.0 σ, number of bins: 100, accepted empty bins: 70%), drop–outs (percentile defining

197   extreme bins: 10, accepted central drop–outs: 10%, accepted extreme drop–outs: 6%), absolute

198   limits (-30 m s^{-1} < U < 30 m s^{-1}, -5 m s^{-1} < W < 5 m s^{-1}, -40 °C < Ts < 40 °C, 200 µmol mol^{-1} < CO$_2$

199   < 500 μmol mol^{-1}, 0 μmol mol$^{-1} <$ H$_2$O < 40 μmol mol^{-1}, 0.17 μmol $<$ CH$_4 < 1000$ μmol), Skewness

200   and kurtosis (-2.0 < Skewness lower limit < -1.0, 1.0 < Skewness up limit < 2.0; 1.0 < Kurtosis

201   lower limit < 2.0, 5.0 < Kurtosis upper limit < 8.0), discontinuities (hard–flag threshold: U = 4.0,

202   W = 2.0, T$_S$ = 4.0, CO$_2$ = 40, CH$_4$ = 40, and H$_2$O = 3.26; soft–flag threshold: U = 2.7, W = 1.3, T$_S$

203   = 2.7, CO$_2$ = 27, CH$_4$ = 30, and H$_2$O = 2.2), angle of attack (minimum angle of attack = -30,

204   maximum angle attack = 30, accepted amount of outliers = 10%), and steadiness of horizontal

205   wind (accepted wind relative instationarity = 0.5) (Vickers and Mahrt, 1997; Mauder et al., 2013).

206   2) The data was then corrected using atmosphere physical calculations expressed by: axis

207   rotations of tilt correction (double rotation), time lags compensation (covariance maximization),

208   and compensating density fluctuations of Webb–Pearman–Leuning (Webb et al., 1980). When

209   CO$_2$ and H$_2$O molar densities are measured with the LI–COR 7500 / LI–COR 7500A in cold

210   environments (low temperatures below -10 °C), a correction should be applied to account for the

211   additional instrument–related sensible heat flux, due to instrument surface heating / cooling. Thus,

212   we implemented the correction according to Burba et al. (2008), which involves calculating a

213   corrected sensible heat flux (H') by adding estimated sensible heat fluxes from key instrument

214   surface elements, including the bottom window (H_{bot}), top window (H_{top}), and spar (H_{spar}) to the

215   ambient sensible heat flux (H):

216         $H'=H+ H_{bot}+ H_{top}+0.15 \times H_{spar}$ (2)

217   3) Quality assurance (QA) / quality control (QC) were ensured through spectral analysis

218   and corrections analysis in EddyPro. Spectra and co–spectra calculations used power–of–two

219   samples to speed up the Fast Fourier Transform (FFT) algorithm. Here we checked the "Filter

220   (co)spectra according to Vickers and Mahrt (1997) test results" box in EddyPro, which would then

221   disregard EC flux time series that would likely create artifacts in spectral and co-spectral shapes.

222   We also used the Mauder and Foken (2004) micrometeorological quality tests embedded in

223   EddyPro to filter low quality EC time series data. Low–frequency range spectral correction was

224   done considering high–pass filtering effects. High–frequency range spectral correction was done

225   considering low–pass filtering effects (Moncrieff et al., 2004).

226   4) We chose values of "0",”1”, "2" to flag the processed flux data into three quality classes

227   in EddyPro. The combined flag attains the value "0" for best quality fluxes, "1" for fluxes suitable

228   for general analysis, such as annual budgets, and "2" for fluxes that should be discarded from the

229   results dataset. For our dataset, approximately 67% of the data fell into Class 0, 12% in Class 1,

230   and 21% in Class 2.

231   5) Our analysis indicated that, under average meteorological conditions, 80% of the flux

232   (footprint) came from an area within 175 m of the eddy covariance tower.

233   In addition, we also adopted the method in Burba et al. (2008) to adjust the half–hour flux

234   data, to avoid apparent measurement errors. In doing this, we rejected half–hour flux data that fell

235   into one of the following situations: (1) incomplete half–hour measurements, (2) measurements

236   under rain impacts, (3) nighttime measurements under stable atmospheric conditions (friction

237   velocity $U^* < 0.1$ m s^{-1}), and (4) abnormal values detected by a three–dimensional ultrasonic

238   anemometer. This screening resulted in the rejection of about 20.7% of all the flux data.

239   After the above data quality control, there was a 28.7% data gap for CH_4 fluxes over the

240   entire period. These data gaps were then filled according to the method described in literature

241   (Falge et al., 2001; Papale et al., 2003). We used a linear interpolation to fill the gaps if they were

242   less than 2 hours, a method described in Falge *et al*. (2001) to fill gaps greater than 2 hours, but

243 less than 1 day, and an artificial neural network approach as described in Papale et al. (2003) and

244 Dengel et al. (2013) to fill gaps greater than 1 day.

245   The quality of the dataset was evaluated using the equation of energy closure:

246
$$EBR = \sum (H + \lambda E) / \sum (R_n - G - S) \qquad (3)$$

247   where the *EBR* is surface energy balance ratio, *H* is heat flux, λE is latent heat, *Rn* is net

248 radiation, *G* is soil heat flux (SHF), and *S* is heat storage of the vegetation canopy. As vegetation

249 coverage at this research site is sparse, *S* is ignored. From 2012 to 2016, the average *EBR* value at

250 the Beilu'he EC site was about 0.675, falling within the range of 0.34 to 1.69 in an analysis of

251 energy balance closure for global FLUXNET sites (Wilson et al., 2002).

252   We analyzed two different major sources of CH_4 flux gap–filling uncertainty. The first kind

253 of uncertainty came from U* threshold estimate. Following Burba et al. (2008), we excluded the

254 probably false low CH_4 flux at low U*. However, it was difficult to determine the value for the

255 U* threshold. For instance, when choosing a lower U* threshold, the associated lower flux would

256 contribute to the gap filling and the annual gross (Loescher, et al., 2006). Here we used the variance

257 from 5% to 95% of the bootstrapped values to provide an estimate on the uncertainties caused by

258 different U* thresholds. The second uncertainty source was due to insufficient power supply. In

259 this research, all instrument power was supplied by solar panels. Extended periods of rainy, cloudy,

260 and snowy weather would cause the instrument to stop working due to an insufficient power supply.

261 When we used the gap-filling method mentioned above, it would cause the CH_4 flux to deviate

262 from the true value. To our knowledge, the CH_4 flux data was largely uncertain under rainy

263 conditions.

2.6 New classification system of the four seasons based on microbial activities classification

264

265   We redefined the four seasons of spring, summer, autumn, and winter based on the

266   microbial activity parameters of the new seasons (Figure 2), ALT variability coefficients (ALT

267   variability coefficient $= (ALT_{i+1} - ALT_i) / ALT_{Max}$, where ALT_{Max} is the maximum of ALT per

268   year), and T_{soil}. Below, we describe the start date of each season (the end date of a season is the

269   day immediately before the start of the next season).

270   Spring starts at the first day of two consecutive observation periods fulfilling both (1) ($\Delta II +$

271    $\Delta I) / 2 \geqslant 15\%$, and (2) the ALT variability coefficient $\geqslant 0.05$.

272   Summer starts on the first day of two consecutive observation periods when (1) ($\Delta II + \Delta I$) /

273    $2 \geqslant 45\%$, (2) ALT variability coefficient $\geqslant 0.35$, and (3) five successive days with T_{soil} at 40

274   cm soil depth $\geqslant 0\,°C$.

275   Autumn starts on the first day of two consecutive observation periods when (1) ($\Delta II + \Delta I$) /

276    $2 \geqslant 55\%$, (2) the ALT variability coefficient $\geqslant 0.60$, and (3) five successive days the T_{soil} of 10

277   cm $< 5\,°C$.

278   Winter starts on the first day of two consecutive observation periods that (1) ($\Delta II + \Delta I$) / 2

279    $< 15\%$ and the ALT variability coefficient < 0.05.

280   To test the robustness of our new seasonal division method in our methane cycle analysis,

281   we compared empirical CH_4 flux estimates using different season definitions (Table 2). In

282   addition to our new method that was based on top soil microbe activity, T_{soil} of $0 - 40$ cm, and

283   permafrost active layer variability (hereafter refer to as SMT), we also used three conventional

284   methods, based on (i) vegetation cover and temperature change (VCT), (ii) based on Julian

13

285   months (JMC), and (iii) based on vegetation phenology change (VPC). The VCT method splits a

286   year into a plant growing season and a non–growing season; the JMC method assumes May to

287   October as a plant growing season, and November to the following April as a non–growing

288   season; and the VPC method defines a plant growing season as the period between the time when

289   all dominant grass species (*Carex moorcroftii* Falc. *ex* Boott, *Kobresia tibetica* Maxim,

290   *Androsace tanggulashanensis*, *Rhodiola tibetica*) germinate and that when they all senesce.

291   **2.7 Statistical Analyses**

292   To understand the connections between CH_4 fluxes and associated environmental factors,

293   we performed a series of statistical analyses, including correlation, principal component analyses

294   (PCA), and linear regression analyses, in IBM SPSS (IBM SPSS Statistics 24; IBM, Armonk

295   NY, USA). Specifically, we used bivariate correlation to examine pairwise relationships between

296   environmental factors and CH_4 fluxes. We also used PCA and linear regressions to explore the

297   sensitivity of CH_4 fluxes to simultaneous environmental fluctuations in wind speed, T_{air}, air

298   relative humidity, Rn, vapor pressure deficit (VPD), albedo, SHF, SWC, and T_{soil}. Before

299   performing PCA and linear regressions, the entire dataset was examined for outliers (Cook's

300   Distance, < 0.002), homogeneity of variance (Levene test, $p < 0.05$), normality (Kolmogorov–

301   Smirnov test, smooth line for histogram of Studentized residuals), collinearity (variance inflation

302   factor, $0 < VIF < 10$), potential interactions (*t*–test, $p < 0.05$), and independence of observations

303   (*t*–test, $p < 0.05$).

304   We performed structural equation modeling (SEM) to evaluate the effects of

305   environmental variables on CH_4 fluxes for different seasons. SEM is a widely-used multivariate

306   statistical tool that incorporates factor analysis, path analysis, and maximum likelihood analysis.

307   This method uses *priori* knowledge of the relationships between focus variables to verify the

308 validity of hypotheses. Here we performed SEM analyses with AMOS 21.0 (Amos Development

309 Corporation, Chicago, IL, USA). All data are presented as mean values with standard

310 deviations.

311 **3. Results**

312 **3.1 Meteorological Conditions**

313   We first reported the statistics of the meteorological conditions at the Beilu'he Permafrost

314 Weather Station between 2012 to 2016. Mean annual T_{air} was -4.5 ℃ (Supplementary Figure 1),

315 with minimum and maximum mean diel temperatures of -21.6 ℃ (12th January, 2012) and 13.8 ℃

316 (28th July, 2015), respectively. Average net radiation was 82.8 Wm^{-2}, with the maximum in August

317 (136.2 Wm^{-2}; Supplementary Figure 2). The average VPD was about 0.3, with maximum and

318 minimum values of 0.98, and 0.02, respectively (Supplementary Figure 3). Mean annual

319 precipitation was 335.4 mm (Figure 3), which was primarily based on rain and snowfall (only

320 occupied 7%). Maximum and minimum precipitation was encountered in 2013 (488.3 mm), and

321 2015 (310.0 mm), respectively. The majority of precipitation, approximately 92%, occurred

322 hereby in the summer. During the winter, precipitation was rare with mean values around 6.7 mm.

323 Spring was another important rainfall period besides summer, with mean precipitation being about

324 37.5 mm, or 8～17% of the total.

325   The Beilu'he site is windy during most of the year (Supplementary Figure 4). Its annual

326 average speed was 4.4 m s^{-1} from 2012 to 2016, while the principal direction of the strongest winds

327 were from the southwest. Late autumn, winter, and early spring drought brought increased risks of

328 dust blowing days, with an average of 122 days within a year. Its summer average wind speed was

329 about 3.30 m s^{-1}, predominantly driven by the southwest wind.

330   The SWC and T_{soil} variability from 2012 to 2016 at the field site are summarized in

331   Supplementary Figures 5 and 6, respectively. Mean SWC of depths 10 cm, 20 cm, 40 cm, 80 cm,

332   and 160 cm were 14%, 9%, 8%, 14%, and 19%, respectively. T_{soil} of depths <100 cm corresponded

333   with the T_{air} changes, but showed stronger differences at depths >100 cm. The T_{soil} at 200 cm depth

334   showed a remarkable difference from that of other layers. The reason could be the occurrence of

335   peat in this layer, and that, during winter, the peat layer was not completely frozen. Supplementary

336   Figure 7 shows SHF half-hour and diel scale variability of 5 cm and 15 cm depth. The annual mean

337   value of SHF at 5 cm and 15 cm depth is 7.6 W m^{-2} and 6.8 W m^{-2}, respectively.

338   Finally, Supplementary Figure 8 shows the site's average soil freezing and thawing

339   dynamics observed from January 2012 to December 2016. The average ALT is 4.4 m from 2012

340   to 2016. At 40 cm depth the duration of the active layer ranged from 174 to 188 days, with an

341   average variation of up to 14 days.

342   **3.2 Annual, Seasonal and Diel Variabilities of Methane Fluxes**

343   Our results indicated that the Beilu'he site was a CH_4 sink, with an annual mean strength

344   of -0.86 ± 0.23 g CH_4–C m^{-2} (95% confidence interval; negative values mean CH_4 sinks, positive

345   values mean CH_4 sources). The strength of the CH_4 sink varies across different years from -0.57

346   ± 0.27g CH_4–C m^{-2} yr^{-1} in 2015, to -1.49 ± 0.38g CH_4–C m^{-2} yr^{-1} in 2014 (Figure 3). The amount

347   of gene expression by methanogens and methanotrophs at 0 − 25 cm soils in March and

348   November, for instance, were about 16.8% and 35.6%, respectively, suggesting strong microbial

349   activities even during the cold and dry plant non–growing season (Figure 2).

350   We also clearly observed CH_4 seasonal variations (Supplementary Figure 9) in both the

351   amount of CH_4 exchanges and their diel cycles (Figure 4). Across different seasons the footprint

16

352   of the monitored CH_4 flux changed following the change of the prevalent wind direction. In

353   winter and spring, the major footprint was from east of the EC tower; while in summer and

354   autumn, the major footprint was from the EC tower's west and north (Supplementary Figure 4).

355   In winter, the net CH_4 flux at the Beilu'he site was an atmospheric source, with an

356   average annual rate of 0.41 ± 0.16 g CH_4–C m^{-2} yr^{-1} or 4.35 ± 0.33 mg CH_4–C m^{-2} d^{-1}

357   (Supplementary Figure 9a). It should also be noted that since the investigation started January 1st,

358   2012, and ended on December 31st, 2016, the 2011 ～ 2012 and 2016 ～ 2017 winters were only

359   about half of the regular length. The diel CH_4 cycle of an average winter day was characterized

360   by one single emission peak around 10:30am ～ 17:30 pm (Figure 4a1-4f1).

361   In spring, the Beilu'he site was a CH_4 source of 0.90 ± 0.37 g CH_4–C m^{-2} yr^{-1}

362   (Supplementary Figure 9b), accounting for 53% of annual CH_4 emissions, or 1.81 ± 0.22 mg

363   CH_4–C m^{-2} d^{-1}. For a typical spring day (Figure 4a2-4e2), diel CH_4 emission usually started at

364   around 10:00 am ～ 10:30 am, when the thin ice layer on the soil surface started to thaw. It then

365   reached the peak at 12:30 pm ～ 13:30 pm. The emission peak started to weaken at around 15:30

366   pm ～ 16:00 pm and reached around zero or even turned into a small sink after 20:00 pm.

367   In summer, the Beilu'he site was a CH_4 sink of -0.99 ± 0.18 g CH_4–C m^{-2} yr^{-1}

368   (Supplementary Figure 9 c), or -13.28 ± 0.38 mg CH_4–C m^{-2} d^{-1}. The diel cycle of CH_4 fluxes in

369   summer was characterized with two absorption peaks and one small emission peak (Figure 4a3-

370   4e3). With T_{air} increasing after sunrise, the soil started to absorb atmospheric CH_4 and this soil

371   uptake process reached its first peak at around 9:30 am ～ 10:30 am. After that, the continuously

372   increasing T_{air} turned to suppress CH_4 uptake and promote CH_4 emissions, likely due to different

373   temperature sensitivities of methanotrophic and methanogenic bacteria. At around 15:30pm ～

374   16:00 pm, when T_{air} reached the maximum (Supplementary Figure 1b), CH_4 emission also

375   reached its peak. The following temperature decrease in the late afternoon again reversed the

376   CH_4 uptake / emission process, and by sunset we observed another CH_4 sink peak. The rate of

377   CH_4 sink then decreased again through the night with further decreasing temperature.

378   Autumn was another season with a net CH_4 sink, with the season having the highest

379   observed value for the site as a CH_4 sink in 2013 (Supplementary Figure 9d). The CH_4 sink in

380   autumn varied between -0.69 ± 0.19 g CH_4–C m^{-2} (2015), and -1.59 ± 0.33 g CH_4–C m^{-2} (2013),

381   with an average diel rate of -1.19 ± 0.48 g CH_4–C m^{-2} yr^{-1} or -13.31 ± 0.28 mg CH_4–C m^{-2} d^{-1}.

382   The diel dynamics of autumn CH_4 fluxes was like a letter "V", with a single sink peak during

383   13:30 pm $\sim$ 15:30 pm (Figure 4a4-4e4).

3.3 Response of Methane Fluxes to Changes in Environmental Factors

385   Diel fluxes of CH_4 were correlated with many biotic and abiotic environmental factors,

386   either positively or negatively (Table 3). Positive factors include metagenomics of both

387   methanotrophic (r = 0.52, $p < 0.01$) and methanogens (r = 0.49, $p < 0.01$) at $0 - 25$ cm soils,

388   ALT (r = 0.43, $p < 0.01$), and wind speed (r = 0.15, $p < 0.01$). Important negative factors include

389   VPD (r = -0.26, $p < 0.01$), SWC at all depths (varied r values between -0.17 and -0.26, $p < 0.01$),

390   T_{air} (r = -0.11, $p < 0.01$), and air pressure (r = -0.15, $p < 0.01$). The correlation signal between

391   CH_4 fluxes and T_{soil} changed with soil depths (varied r values between -0.09 and 0.24, $p < 0.01$).

392   Furthermore, path analysis results showed that T_{soil} at 5cm and 10cm were the most important

393   factors, which together contributed about 25% of the relative importance coefficient. Following

394   these factors in importance were SWC at 80 cm (14%) and 20 cm (12%), and T_{soil} at 20 cm (8%).

395   Further analyses suggested that dominant control factors of CH_4 fluxes also changed

396   among different seasons. In spring, Rn was the most important factor, with a relative importance

397   coefficient near 60%, followed by SHF at 5 cm (9%), and SWC at 20 cm (6%). Table 4 shows

398   the results of the PCA. In spring, PC1 explained 63% of the CH_4 variations, which was

399   positively correlated with T_{air}, VPD, Rn, SHF of 15 cm, ALT, ΔI, SWC of $10 - 40$ cm, T_{soil} of 0

400   cm, T_{soil} of $5 - 20$ cm, T_{soil} of $30 - 50$ cm, and negatively correlated with wind speed. The PC2

401   explained about 23% of CH_4 fluxes variations. The first four principal components explained

402   about 86% of the CH_4 variations.

403   In summer, CH_4 fluxes were mostly related with T_{soil} at 100 cm and 200 cm, with a

404   relative importance coefficient of about 30.2% and 26.5%, respectively. Other important

405   environmental determinants of CH_4 fluxes were T_{soil} at 70 cm (12.3%), and T_{soil} at $0 - 20$ cm

406   (11.4%). The first four principal components explained about 88% of the CH_4 variations (Table

407   4). PC1 explained 70% of the CH_4 variations and was positively correlated with wind speed, T_{air},

408   VPD, SHF of 15 cm, ALT, ΔI, SWC of $50 - 160$ cm, precipitation, T_{soil} of 0 cm, T_{soil} of $5 - 40$

409   cm, T_{soil} of $50 - 80$ cm, and T_{soil} of $100 - 200$ cm, but negatively correlated with Rn and SWC of

410     $10 - 40$ cm.

411   In autumn, Rn and T_{soil} at $5 - 20$ cm had the highest relative importance coefficients for

412   explaining the CH_4 flux variation. The first four principal components explained about 86% of

413   the CH_4 variations (Table 4). PC1 explained 69% of the CH_4 variations and was positively

414   correlated with T_{air}, VPD, Rn, SHF of 15 cm, ALT, ΔI, SWC of $10 - 40$ cm, SWC of $50 - 160$

415   cm, T_{soil} of 0 cm, T_{soil} of $5 - 40$ cm, T_{soil} of $50 - 80$ cm, and T_{soil} of $100 - 200$ cm, but negatively

416   correlated with wind speed.

417   During winter, Rn was again the most important factor (34% relative importance

418   coefficient), followed by T_{soil} at $0 - 40$ cm (27% in total), and SHF of 15 cm (17% in total), in

419   determining CH_4 fluxes. The first four principal components explained about 96% of the CH_4

420   variations (Table 4). PC1 explained 75% of the CH_4 variations and was positively correlated

421   with wind speed, T_{air}, VPD, Rn, SHF of 15 cm, ΔI, T_{soil} of 0 cm, and T_{soil} of $5 - 20$ cm.

422   **3.4 Empirical Model Comparison for Different CH_4 Flux Season Classification System**

423   Lastly, we also compared how different season definitions, including the methods of

424   SMT, VCT, JMC, and VPC, may have impacted the predictbility of CH_4 fluxes. We established

425   empirical maximum likelihood models between all environmental factors and diel CH_4 fluxes

426   over each season, and then compared modeled CH_4 fluxes and field observations under those

427   methods of different seasonal definitions (Figure 5). We found that the agreement between

428   modeled and observed CH_4 fluxes, using the new SMT method, reached $R^2 = 0.28$, almost twice

429   that of the VPC ($R^2 = 0.17$) and VCT ($R^2 = 0.14$) methods, and more than three times that of the

430   JMC method ($R^2 = 0.08$; Figure 5). Hence, the comparison suggested that our new method could

431   better model CH_4 fluxes over a year. The use of the traditional plant growing season versus

432   nongrowing season definitions may also underestimate or overestimate CH_4 sinks or sources,

433   especially when many studies assume CH_4 is close to zero during the plant nongrowing season.

434   Furthermore, the new SMT method accurately captures the impact of spring and autumn

435   permafrost thawing / freezing cycles on CH_4 fluxes, and the different preferable environments

436   for methanogens and methanotrophic bacteria during the summer season, while conventional

437   methods do not.

438   **4. Discussion**

4.1 Annual, Season mean and Diel Variability

Our results suggested that the alpine steppe ecosystem in Beilu'he was a CH4 sink of about -0.86 ± 0.23 g $CH_4 - C$ m^{-2} yr^{-1} during the study period of 2012-2016. This sink strength is larger than that of previous reports from other sites of the QTP (Cao et al., 2008; Wei et al., 2012; Li et al., 2012; Song et al., 2015; Chang and Shi, 2015), and many other high-latitude Arctic tundra ecosystems, like northeast Greenland (Jørgensen et al., 2015), western Siberia (Liebner et al., 2011), and Alaska (Whalen et al., 1992; Zhuang et al., 2004; Whalen, 2005). Different soil hydrothermal conditions, which previous studies have shown will greatly influence CH_4 cycles in permafrost regions (Spahni et al., 2011; Kirschke et al., 2013), may partly explain the site difference in CH_4 dynamics. For example, compared to the wet and often snow–covered high–latitude Arctic tundra ecosystems, there is no or little snow cover during the cold season in the QTP alpine steppes (Supplementary Table 1). During winter, the Beilu'he meteorological data shows that the snow-cover time < 33.7h, SWC of 0-40cm within footprint $< 7.6\%$ from 2012 to 2016 (Supplementary Table 1) , is far below high–latitude Arctic tundra ecosystems. Jansson and Taş (2014) pointed out that relatively dry soils could faciliate the oxidation of CH_4, since the increased number of gaps between soil particles in dry soils enhances the diffusion of oxygen (O_2) and CH_4 molecules and promotes aerobic respiration of soil microorganisms (Wang et al., 2014; Song et al., 2015). Meanwhile, unfrozen or capillary water found in cold–season permafrost soils ensures sufficient soil moisture for microbial activities, even in relatively drier and cold soils (Panikov and Dedysh, 2000; Rivkina et al., 2004). In addition, many previous studies used static chambers in CH_4 measurements, and may not have included a plant non– growing season (Wei et al., 2015a; Wang et al., 2014). Static chambers could underestimate CH4

461 uptake because of the additional chamber heating-induced CH_4 emissions and frequent

462 measurement gaps from overheating preventive shutdowns (Sturtevant et al., 2012).

463   We argued that seasonal freezing and thawing dynamics may be a key reason to explain

464 the site's seasonal difference in CH_4 dynamics. Freezing and thawing processes are typical

465 characteristics of the QTP permafrost (Wang et al., 2008; Wang et al., 2000; Qin et al., 2016).

466 Our work suggests that freezing and thawing dynamics have played a critical role in governing

467 permafrost seasonal and diel CH_4 cycling. For instance, while both spring and autumn are active

468 seasons for the freeze-thaw dynamics of top soil layers and share many similarities, they have

469 opposite CH_4 processes–soils emit CH_4 during spring (Supplementary Figure 9 b), but consume

470 CH_4 during autumn (Supplementary Figure 9d). We hypothesize that the difference in the

471 freezing and thawing processes of the two seasons may have played a critical role in determining

472 the direction of CH_4 dynamics. In spring, the SWC of 10 cm, of 20-40 cm of 80 cm, and of 160

473 cm depth is 12.4%, 9.2%, 11.4%, and 13.6%, respectively (Supplementary Table 1). The active

474 soil layer thaws from top to bottom (Jin et al., 2000; Cao et al., 2017), and the permafrost table is

475 very shallow (about 10 $\sim$ 45 cm) and often water proof (Wu and Zhang, 2008; Song et al., 2015;

476 Lin et al., 2015). The water thawed during the day time would freeze again at night on the soil

477 surface (Supplementary Figure 10a; Shi et al., 2006; Wu and Zhang, 2010b). The thin-ice layer

478 could stop atmospheric gases of CH_4 and O_2 from getting into the soils (Gazovic et al., 2010).

479 During autumn, the SWC is 15.3% at 10 cm below ground, decreases to 9.4% at 20-40 cm, and

480 then increases to 13.6% and 21.0% at 80 cm and 160 cm, respectively (Supplementary Table 1).

481 However, soils are bi-directionally frozen from both top (ground surface) and bottom

482 (permafrost table) which is about 200~400 cm below ground (Supplementary Figure 8; Wu and

483 Zhang, 2010a). On the one hand, the frozen soil of the ground surface (about 0-40cm) prevents

484   the outside liquid water from permeating. On the other hand, the freezing itself will reduce the

485   liquid water content in the soil. Therefore, it creates finely closed anaerobic gaps that allow CH_4

486   and O_2 gases into deep soils (about 50~400 cm; Mastepanov et al., 2008; Mastepanov et al.,

487   2013; Zona et al., 2016). Meanwhile, the temperature of deep soils (about 50~400 cm) still

488   remains at a relatively high level (Supplementary Figure 10b), and methanotrophic bacteria will

489   still be active at this high T_{soil} (Figure 2). This could be one important mechanism for autumn

490   soil CH_4 consumption. In addition, in principal it is also possible that the observed seasonal

491   variation in CH_4 flux may actually arise from the spatial variation of the footprint covered by the

492   eddy covariance site (within 175 m), given that prevalent wind direction changes seasonally

493   (Supplementary Figure 4). Nonetheless, we found that the same vegetation species and soil exist

494   in different directions to the tower within the footprint (Supplementary Figure 11). This spatial

495   vegetation and soil homogeneity rules out the potential influence of footprint changes on the sign

496   of CH_4 balances, and further confirms that seasonal soil freezing and thawing differences may

497   likely be the main explanation for seasonal CH_4 variations.

498   Furthermore, we suggested that the specific autumn soil vertical structure may help to

499   explain why the site was a CH_4 sink, unlike the CH_4 source in spring. The sequential probing

500   data enables us to establish a rough estimate on the soil vertical structure during the autumn

501   thawing–freezing process, in which the vertical distribution of clay, sandy soils, and soil organic

502   layers was mixed like a multi–layer hamburger structure, rather than forming a gradual change

503   (Figure 6e). As the soil profile is vertically different in features such as soil density, thermal

504   conductivity, latent heat, soil salinity, we boldly conjecture that the T_{soil}, SWC, and soil

505   microbial activities also had this hamburger type of vertical distribution in a similar way. As a

506   result, layers of frozen and thawed soils were not changing gradually but appeared like a

507   hamburger structure too. This soil vertical structure trapped high concentrations of soil water

508   between the frozen layers, which was therefore highly anaerobic and suitable for CH_4

509   production. It may also allow speculation that biogenic CH_4 between frozen layers could not

510   escape in autumn. The biogenic CH_4 would be trapped until the active soil layer was completely

511   frozen in late autumn, and in some warmer years until early winter and created frost cracks. This

512   would enable it to escape and may explain why there was a large burst of CH_4 emissions in late

513   autumn and early winter and may also explain the constantly weak CH_4 emission through the

514   winter season, although methanogenic bacteria may have stopped functioning in the low

515   temperature of winter. Of course, further studies and direct data collection in the field will be

516   needed to fully test the hypothesis.

517   **4.2 Impacts of Environmental, Permafrost, and Microbial Activities on CH_4 Fluxes**

518   Our results demonstrated the important roles of climate, freezing and thawing dynamics,

519   and soil microbe activities in regulating the direction and amount of CH_4 exchanges between the

520   atmosphere and ecosystems in permafrost areas. The key role of the above factors and processes

521   was also confirmed by the better representation of seasonal CH_4 cycles by our new seasonal

522   division method based on soil microbes, temperature, and permafrost dynamics rather than T_{air} or

523   vegetation phenology. Here, we further discuss potential mechanisms of how environmental

524   (including air and soil heat and water), freezing and thawing processes, and soil microbes control

525   the production and absorption of CH_4.

526   First, it is noteworthy that both the strength and direction of correlations between CH_4

527   fluxes, SWC, and T_{soil} parameters changed with soil depths, particularly during spring and

528   autumn, when active layer soils shifted between thawing and freezing regularly. The positive and

529   negative CH_4 flux correlations with T_{soil} and SWC may suggest that the impacts of T_{soil} and SWC

530   on CH$_4$ fluxes shall be treated as a holistic process (Table 3), rather than as separate ones. For

531   instance, in autumn, the significant correlation between CH$_4$ fluxes and T$_{soil}$ or SWC was

532   positive at some soil depths, but negative at some other depths, reaching the maximum at the

533   depth of 80 cm. Further, *in situ* observations suggested that soil organic matter and soil microbe

534   amount were also at a very high level at this depth, highlighting that the regulation of soil abiotic

535   factors on CH$_4$ cycling may be well influenced by soil biotic activities. In addition, the holistic

536   soil heat–water process could also determine the concentration of soil inorganic ions, particularly

537   during spring and autumn, which were critical factors controlling the amount of soil unfrozen

538   water. Earlier studies suggested that soil unfrozen water is important for maintaining soil

539   microbial activities in winter (Panikov and Dedysh, 2000; Rivkina et al., 2004). In the future we

540   will include data acquiring of soil unfrozen water to test its role in regulating CH$_4$ exchanges in

541   permafrost regions.

542   T$_{air}$ and precipitation impact CH$_4$ fluxes indirectly through their influences on T$_{soil}$ and

543   SWC (Zhuang et al., 2004; Lecher et al., 2015). Such indirect influences may often be

544   characterized with time–lagged effects (Koven et al., 2011). For instance, post–drought rainfall

545   events in summer can first promote soil CH$_4$ consumption (summer of 2014). This is because

546   certain soil moisture is needed for methanogenic bacteria to function (Del et al., 2000; Luo et al.,

547   2012). Yet, prolonged rainfall will eventually cause CH$_4$ fluxes to change from negative (soils

548   consume CH$_4$) to positive (soils emit CH$_4$) fluxes (for example, day 168 to 183 of 2015, Figure

549   3d). After rainfall events, CH$_4$ flux gradually turned negative again with the decrease of SWC.

550   As a result of these time–lagged effects, the correlation coefficient between CH$_4$ fluxes and

551   precipitation often appears very low, although still statistically significant.

552   Second, soil methanogenic and methanotrophic bacteria could co–exist with different

553   optimal niches (e.g., ranges of T_{air} / T_{soil} and SWC; Zhuang et al., 2013; Lau et al., 2015; Wei et

554   al., 2015a). For example, the CH_4 diel cycle in summer was found to have two strong

555   consumption peaks and one weak emission peak (Figure 4: a3, c3, d3, e3). The timing of these

556   different peaks may well reflect the different environmental requirements for the dominance of

557   methanogens and methanotrophic bacteria. Furthermore, methanogens may have a broader

558   functional temperature range than methanotrophic bacteria (Kolb, 2009; Lau et al., 2015; Yang et

559   al., 2016). This is also evident, for example, from the diel CH_4 cycle in autumn when CH_4

560   consumption was minimal at both lowest and highest T_{air} (Figure 4a4-4e4).

561   The complex relationships between CH_4 fluxes and environmental factors make it a grand

562   challenge to predict the future of the QTP CH_4 budget under a changing climate. For instance, it

563   has been generally believed that the ALT will increase under projected warming (Wu and Liu,

564   2004). The positive correlation between CH_4 fluxes and ALT found here suggests that the QTP

565   permafrost CH_4 sink may thus be weakened. However, the negative correlation between CH_4

566   flux and T_{air} may lead to a different conclusion. Incorporating our findings and high–resolution

567   data into mechanistic CH_4 models is therefore needed to enhance our capacity in predicting

568   future CH_4 budgets. Earth system models have been introduced to estimate CH_4 dynamics

569   (Curry, 2007; Spahni et al., 2011; Bohn et al., 2015). For example, using a terrestrial ecosystem

570   modelling approach, Zhuang et al. (2004) estimated the average QTP permafrost CH_4 sink of -

571   0.08 g C m^{-2} yr^{-1}, much smaller than our field–based CH_4 estimate (-0.86 $\pm$ 0.23 g CH_4–C m^{-2} yr^{-}

572   ^{1}). Current CH_4 models focus on the regulation of CH_4 processes by temperature and SWC, and

573   usually lack high–resolution data for model parameterization (Bohn et al., 2015). Data

574   interpolation and the use of average values of certain environmental factors are normal practices

575   in most models (Zhuang et al., 2004), which may overlook the impacts of environmental

576   variations on CH_4 dynamics. For example, at Beilu'he, T_{air} on a typical summer day (e.g., July

577   6th, 2013) could vary between -6 °C and 28 °C, a difference of 34 °C. The resulting diel mean

578   temperature, 17 °C, is beyond the range of methanotrophic bacteria's preferable temperature of

579   20～30 °C (Segers, 1998; Steinkamp et al., 2001; Yang et al., 2016). Therefore, models using

580   diel mean temperature as an input may estimate the site as a net CH_4 sink. However, field

581   observations show a source with a sink only during a short period (8:30am～11:30 am), on July

582   6th, 2013, because the short period of the sink was offset by the source over the remaining 21

583   hours.

584   Furthermore, half–hourly SWC was well related with the waterproof role by the

585   permafrost layer during spring and autumn (Figure 6a). However, because of the shortage of high

586   temporal resolution data, half–diel or diel mean SWC data are often used in many previous

587   studies (Zhu et al., 2004; Jiang et al., 2010; Wei et al., 2015b), which could not correctly show

588   the regulation of permafrost soil properties that are critical for CH_4 dynamics. As another

589   example, T_{soil} of $0 - 50$ cm depth is one of the most important factors related to CH_4 fluxes

590   (Mastepanov et al., 2008). However, many studies used T_{air} or re–analyzed deep T_{soil} instead

591   (Zhu et al., 2004; Bohn et al., 2015; Oh et al., 2016). Because the active layer is not

592   homogeneous, but with different thermal conductivities during the freezing and thawing process,

593   the use of T_{air} or deep T_{soil} brings in large uncertainties in CH_4 modelling. Future research needs

594   to improve mechanistic understanding of CH_4 dynamics and their biotic and abiotic control

595   factors, and to conduct more high–resolution and long–term field monitoring.

4.3 The Classification System of the Four Seasons for CH4 Studies

596

597   Our study differs also from the majority of earlier studies regarding the definition of the

598   seasons (Treat et al., 2014; Wang et al., 2014; Wei et al., 2015a; Song et al., 2015). Here, we

599   adopted a new classification system of the four seasons based on $0-25$ cm soil depth bacterial

600   activities (Figure 2), T_{soil} of $0-40$ cm (Supplementary Figure 6a), and ALT (Supplementary

601   Figure 8), rather than the conventional methods based on T_{air} and vegetation dynamics (Chen et

602   al., 2011; McGuire et al., 2012). Previous studies indicated that changes in CH_4 fluxes are

603   regulated by soil microbes, and activities of soil microbes are not limited to the warm season

604   (Zhuang et al., 2004; Lau et al., 2015; Yang et al., 2016). For instance, in March and November,

605   we found the amount of gene expression by methanogens and methanotrophs at $0-25$ cm soils

606   were about 16.8% and 35.6% (Figure 2), respectively, suggesting there are still strong microbial

607   activities during the cold and dry season. Therefore, our new method of defining the four seasons

608   from the top soil biotic and abiotic features better captures the pattern of CH_4 dynamics

609   throughout a year.

5. Conclusions

610

611   Our field data indicates that there was a large CH_4 sink in the QTP permafrost area during

612   recent years. The strength of this CH_4 sink is larger than found in previous studies in the same

613   region and many high–latitude tundra ecosystems. This study highlights the complexity of

614   environmental controls, including soil heat–water processes, permafrost freezing and thawing

615   dynamics, and soil microbial activities, on CH_4 cycling. This complexity implies that linear

616   interpolation and extrapolation from site-level studies could introduce large uncertainties in CH_4

617   flux estimation. Future quantification of CH_4 dynamics in permafrost regions needs to account

618   for the effects of complex environmental processes. Our findings also highlight the importance

28

619 of conducting more high–resolution and long–term field monitoring in permafrost regions for

620 better understanding and modelling of permafrost CH_4 cycling under a changing climate.

634 **Reference**

635 Bohn T., Melton J., Ito A.: WETCHIMP–WSL: intercomparison of wetland methane emissions

636   models over West Siberia, Biogeosciences, 12, 3321 – 3349, 2015.

637 Burba, G. G., Mcdermitt, D. K., and Grelle, A.: Addressing the influence of instrument surface

638   heat exchange on the measurements of CO_2 flux from open–path gas

639   analyzers. Glob. Change Biol., 14(8), 1854 – 1876, 2008.

640 Cao G., Xu X., and Long R.: Methane emissions by alpine plant communities in the Qinghai–

641   Tibet Plateau, Biol. Lett., 4, 681 – 684, 2008.

642   Cao B., Gruber S., Zhang T.: Spatial variability of active layer thickness detected by ground–

643   penetrating radar in the Qilian Mountains, Western China, J. Geophys. Res. Earth Surf.,

644   122, 574 – 591, 2017.

645   Cate, R. B., and Nelson, L. A.: A simple statistical procedure for partitioning soil test correlation

646   data into two classes, Soil Sci. Soc. Am. J., 35(4), 658 – 660, 1971.

647   Chang R., Miller C., and Dinardo S.: Methane emissions from Alaska in 2012 from CARVE

648   airborne observations, Proc. Natl. Acad. Sci. U. S. A., 111, 16694 – 16699, 2014.

649   Chang S. and Shi P.: A review of research on responses of leaf traits to climate change, Chin. J.

650   Plant Ecol., 39, 206 – 216, 2015.

651   Chen W., Wolf B., and Zheng X.: Annual methane uptake by temperate semiarid steppes as

652   regulated by stocking rates, aboveground plant biomass and topsoil air permeability.

653   Glob. Change Biol., 17, 2803 – 2816, 2011.

654   Curry C.: Modeling the soil consumption at atmospheric methane at the global scale. Glob.

655   Biogeochem. Cycles, 21, 1 – 15, 2007.

656   Dengel S., Zona D., and Sachs T.: Testing the applicability of neural networks as a gap–filling

657   method using CH_4 flux data from high latitude wetlands. Biogeosciences, 10, 8185 – 8200,

658   2013.

659   Del G., Parton W., and Mosier A.R.: General CH_4 oxidation model and comparisons of CH_4

660   oxidation in natural and managed systems, Glob. Biogeochem. Cycles, 14, 999 – 1019,

661   2000.

662 Falge, E., Baldocchi, D., and Olson, R.: Gap filling strategies for defensible annual sums of net

663   ecosystem exchange, Agric. For. Meteorol., 107(1), 43 – 69, 2001.

664 Gažovič M., Kutzbach L., and Schreiber P.: Diurnal dynamics of CH_4 from a boreal peatland

665   during snowmelt. Tellus, B, 62, 133 – 139, 2010.

666 IPCC, climate change 2013: the physical science basis. Contribution of working group I to the

667   fifth assessment report of the intergovernmental panel on climate change., 2013.

668 Jansson, J. K. and Tas, N.: The microbial ecology of permafrost, Nat. Rev. Microbiol., 12, 414,

669   2014.

670 Jiang C., Yu G., and Fang H.: Short–term effect of increasing nitrogen deposition on CO_2, CH_4

671   and N_2O fluxes in an alpine meadow on the Qinghai–Tibetan Plateau, China, Atmos.

672   Environ., 44, 2920 – 2926, 2010.

673 Jin H., Li S., and Cheng G.: Permafrost and climatic change in China, Glob. Planet, Change, 26,

674   387 – 404, 2000.

675 Jørgensen, C. J., Johansen, K. M. L., and Westergaard–Nielsen, A.: Net regional methane sink in

676   High Arctic soils of northeast Greenland, Nat. Geosci., 8, 20, 2015.

677 Kirschke, S., Bousquet, P., and Ciais, P.: Three decades of global methane sources and

678   sinks, Nat. Geosci., 6, 813, 2013.

679 Kolb, S.: The quest for atmospheric methane oxidizers in forest soils, Environ. Microbiol.

680   Rep., 1, 336 – 346, 2009

681 Koven C.D., Ringeval B., and Friedlingstein P.: Permafrost carbon–climate feedbacks accelerate

682   global warming, Proc. Natl. Acad. Sci. U. S. A., 108, 14769 – 14774, 2011.

683   Lau M., Stackhouse B.T., and Layton A.C.: An active atmospheric methane sink in high Arctic

684   mineral cryosols. ISME J., 9, 1880 – 1891, 2015.

685   Lecher A.L., Dimova N., and Sparrow K.J.: Methane transport from the active layer to lakes in

686   the Arctic using Toolik Lake, Alaska, as a case study, Proc. Natl. Acad. Sci. U. S. A., 112,

687   3636 – 3640, 2015.

688   Lee, X., Massman, W., and Law, B. (Eds.): Handbook of micrometeorology: a guide for surface

689   flux measurement and analysis (Vol. 29), Springer Science and Business Media, 2006.

690   Li K., Gong Y., and Song W.: Responses of CH_4, CO_2 and N_2O fluxes to increasing nitrogen

691   deposition in alpine grassland of the Tianshan Mountains, Chemosphere, 88, 140 – 143,

692   2012.

693   Liebner S., Zeyer J., and Wagner D.: Methane oxidation associated with submerged brown

694   mosses reduces methane emissions from Siberian polygonal tundra, J. Ecol., 99, 914 – 922,

695   2011.

696   Lin Z., Burn C.R., and Niu F.: The Thermal Regime, including a Reversed Thermal Offset, of

697   Arid Permafrost Sites with Variations in Vegetation Cover Density, Wudaoliang Basin,

698   Qinghai–Tibet Plateau. Permafr. Periglac. Process., 26, 142 – 159, 2015.

699   Loescher, H. W., Law, B. E., and Mahrt, L: Uncertainties in, and interpretation of, carbon flux

700   estimates using the eddy covariance technique. J. Geophys. Res. Atmos., 111(D21), 2006.

701   Luo G.J., Brüggemann N., and Wolf B.: Decadal variability of soil CO_2, NO, N_2O, and CH_4

702   fluxes at the Höglwald Forest, Germany. Biogeosciences, 9, 1741 – 1763, 2012.

703   Mastepanov M., Sigsgaard C., and Dlugokencky E.J.: Large tundra methane burst during onset

704   of freezing. Nature, 456, 628 – 30, 2008.

705 Mastepanov, M., Sigsgaard, C., and Tagesson, T.: Revisiting factors controlling methane

706   emissions from high-Arctic tundra, Biogeosciences, 10(7), 5139, 2013.

707 Mauder, M., Cuntz, M., and Drüe, C.: A strategy for quality and uncertainty assessment of long–

708   term eddy–covariance measurements. Agric. For. Meteorol., 169, 122 – 135, 2013.

709 McGuire A.D., Christensen T.R., and Hayes D.: An assessment of the carbon balance of Arctic

710   tundra: Comparisons among observations, process models, and atmospheric inversions,

711   Biogeosciences, 9, 3185 – 3204, 2012.

712 Moncrieff, J., Clement, R., and Finnigan, J.: Averaging, detrending, and filtering of eddy

713   covariance time series. In Handbook of micrometeorology (pp. 7 – 31), Springer

714   Netherlands, 2004.

715 Muller, S. W. Permafrost or permanently frozen ground and related engineering problems, 1947.

716 Oh Y., Stackhouse B., and Lau M.: A scalable model for methane consumption in arctic mineral

717   soils. Geophys. Res. Lett., 43, 5143 – 5150, 2016.

718 Panikov N.S. and Dedysh S.N.: Cold season CH_4 and CO_2 emission from boreal peat bogs (West

719   Siberia): Winter fluxes and thaw activation dynamics, Glob. Biogeochem. Cycles, 14, 1071

720   – 1080, 2000.

721 Papale, D., Reichstein, M., and Aubinet, M.: Towards a standardized processing of Net

722   Ecosystem Exchange measured with eddy covariance technique: algorithms and uncertainty

723   estimation. Biogeosciences, 3(4), 571 – 583, 2006.

724 Patra P.K. and Kort E.A.:Regional Methane Emission Estimation Based on Observed

725 Atmospheric Concentrations (2002 – 2012), J. Meteor. Soc. Japan. Ser. II, 94, 91 – 113,

726 2016.

727 Qin, Y., Wu T., and Li R., Using ERA-Interim reanalysis dataset to assess the changes of ground

728 surface freezing and thawing condition on the Qinghai–Tibet Plateau. Environ. Earth Sci.,

729 75(9): 1-13, 2016.

730 Rigby M., Prinn R.G., and Fraser P.J.: Renewed growth of atmospheric methane, Geophys. Res.

731 Lett.,35, 2 – 7, 2008.

732 Rivkina E., Laurinavichius K., and McGrath J.: Microbial life in permafrost, Adv. Space Res.,

733 33, 1215 – 1221, 2004.

734 Segers R.: Methane production and methane consumptiona–review of processes underlying

735 wetland methane fluxes [Review], Biogeochem., 41, 23 – 51, 1998.

736 Shi P., Sun X., and Xu L.: Net ecosystem CO_2 exchange and controlling factors in a steppe–

737 Kobresia meadow on the Tibetan Plateau. Sci. China Ser. D-Earth Sci., 49, 207 – 218, 2006.

738 Song, W., Wang, H., and Wang, G.: Methane emissions from an alpine wetland on the Tibetan

739 Plateau: Neglected but vital contribution of the non–growing season, J. Geophys. Res.

740 Biogeosci., 120, 1475 – 1490, 2015.

741 Spahni R., Wania R., and Neef L.: Constraining global methane emissions and uptake by

742 ecosystems. Biogeosciences, 8, 1643 – 1665, 2011.

743 Steinkamp R., Butterbach–Bahl K., and Papen H.: Methane oxidation by soils of an N limited

744 and N fertilized spruce forest in the Black Forest, Germany, Soil. Biol. Biochem., 33, 145 –

745 153, 2001.

746   Sturtevant C.S., Oechel W.C., and Zona D.: Soil moisture control over autumn season methane

747   flux, Arctic Coastal Plain of Alaska, Biogeosciences, 9, 1423 – 1440, 2012.

748   Treat C.C., Wollheim W.M., and Varner R.K.: Temperature and peat type control CO_2 and CH_4

749   production in Alaskan permafrost peats, Glob. Chang. Biol. 20, 2674 – 2686, 2014.

750   Vickers, D., and Mahrt, L.: Quality control and flux sampling problems for tower and aircraft

751   data. J. Atmos. Ocean. Technol., 14(3), 512 – 526, 1997.

752   Wang G., Li Y., and Wang Y.: Effects of permafrost thawing on vegetation and soil carbon pool

753   losses on the Qinghai–Tibet Plateau, China, Geoderma, 143, 143 – 152, 2008.

754   Wang S., Jin H., Li S.: Permafrost degradation on the Qinghai–Tibet Plateau and its

755   environmental impacts. Permafr. Periglac. Process., 11, 43 – 53, 2000.

756   Wang Y., Liu H., and Chung H.: Non–growing season soil respiration is controlled by freezing

757   and thawing processes in the summer monsoon-dominated Tibetan alpine grassland. Glob.

758   Biogeochem. Cycles, 28, 1081 – 1095, 2014.

759   Webb E. K., Pearman G. I., and Leuning R.: Correction of flux measurements for density effects due to

760   heat and water vapor transfer. Q. J. Royal Meteorol. Soc., 106, 85 – 100, 1980.

761   Wei D., Ri X., and Wang Y.: Responses of CO_2, CH_4 and N_2O fluxes to livestock exclosure in an

762   alpine steppe on the Tibetan Plateau, China. Plant Soil, 359, 45 – 55, 2012.

763   Wei D., Ri X., and Tarchen T.: Considerable methane uptake by alpine grasslands despite the

764   cold climate: In situ measurements on the central Tibetan Plateau, 2008 – 2013, Glob.

765   Chang Biol., 21, 777 – 788, 2015a.

766   Wei D., Tarchen T., and Dai D.: Revisiting the role of CH_4 emissions from alpine wetlands on

767 the Tibetan Plateau: Evidence from two in situ measurements at 4758 and 4320 m above sea

768   level, J. Geophys. Res. Biogeosci., 120, 1741 – 1750, 2015b.

769 Whalen, S. C. and Reeburgh, W. S.: Consumption of atmospheric methane by tundra

770   soils. Nature, 346, 160, 1990.

771 Whalen S.C.: Biogeochemistry of Methane Exchange between Natural Wetlands and the

772   Atmosphere. Environ. Eng. Sci., 22, 73 – 94, 2005.

773 Whalen S.C., Reeburgh W.S., and Barber V.A.: Oxidation of methane in boreal forest soils: a

774   comparison of seven measures. Biogeochemistry, 16, 181 – 211, 1992.

775 Wilson K., et al.: Energy balance closure at FLUXNET sites. Agr Forest Meteorol., 113: 223-

776   243, 2002.

777 Wu Q. and Liu Y.: Ground temperature monitoring and its recent change in Qinghai–Tibet

778   Plateau, Cold Reg. Sci. Technol., 38, 85 – 92, 2004.

779 Wu Q. and Zhang T.: Recent permafrost warming on the Qinghai–Tibetan Plateau. J. Geophys.

780   Res. Atmos. 113, 1 – 22, 2008.

781 Wu Q.and Zhang T.: Changes in active layer thickness over the Qinghai–Tibetan Plateau from

782   1995 to 2007, J. Geophys. Res. Atmos., 115, D09107, 2010a.

783 Wu Q. Zhang T., and Liu Y.: Permafrost temperatures and thickness on the Qinghai–Tibet

784   Plateau, Glob. Planet. Change, 72, 32 – 38, 2010b.

785 Yang S., Wen X., and Shi Y.: Hydrocarbon degraders establish at the costs of microbial richness,

786   abundance and keystone taxa after crude oil contamination in permafrost environments. Sci.

787   Rep., 6, 37473, 2016.

788 Zhu X., Zhuang Q., and Chen M.: Net exchanges of methane and carbon dioxide on the

789   Qinghai–Tibetan Plateau from 1979 to 2100. Environ. Res. Lett., 10, 85007. 2004.

790 Zhuang Q., Melillo J.M., and Kicklighter D.W.: Methane fluxes between terrestrial ecosystems

791   and the atmosphere at northern high latitudes during the past century: A retrospective

792   analysis with a process–based biogeochemistry model. Glob. Biogeochem. Cycles, 18(3),

793   2004.

794 Zhuang Q., Chen M., and Xu K.: Response of global soil consumption of atmospheric methane

795   to changes in atmospheric climate and nitrogen deposition. Glob. Biogeochem. Cycles, 27,

796   650 – 663, 2013.

797 Zona D., Gioli B., and Commane R.: Cold season emissions dominate the Arctic tundra methane

798   budget. Proc. Natl. Acad. Sci. U. S. A., 113, 40 – 45, 2016.

799

800

801

802

803

804

805

806

807

808   **Table 1**. Soil characteristics at the eddy covariance flux study site

Soil depth cm	Soil type	Gravel content	SOC	Microbial Numbers	pH	DBD	SWC	Total N
		$g\,kg^{-1}$	$g\,kg^{-1}$	$\times 10^4$		$g\,cm^{-3}$	%	$\times 10^3\,mg\,kg^{-1}$
0 − 20	clay	22.3	2.8	3.44	8.7	1.75	18.26	0.87
20 − 50	silty clay	12.6	1.7	3.82	8.4	1.73	11.52	1.02
50 − 120	silt and fine sand	3.4	1.3	3.67	8.4	1.72	12.57	1.18
120 − 160	silt and fine sand	2.8	26.4	5.44	5.1	1.68	24.69	2.46
160 − 200	silt and fine sand	1.6	13.6	4.39	6.8	1.68	22.45	2.03

809   **Note:** Gravel content diameter ≥ 0.5cm. SOC is soil organic content, DBD is dry bulk density,

810   SWC is soil water content, and Total N is total nitrogen content.

811

812 **Table 2.** Measurements of four seasons from 2012 to 2016

	Spring	Summer	Autumn	Winter	Plant growing season	Plant non–growing season
	Period; Total days	Period; Total days	Period; Total days	Period; Total days	Period; Total days	Period; Total days
	Days	Days	Days	Days	Days	Days
2012	50 − 142; 93	143 − 229; 87	230 − 323; 94	1 − 49, 324 − 366; 92	139 − 286; 148[a]	1 − 138, 287 − 366; 218[a]
					122 − 305; 184[b]	1 − 121, 306 − 366; 182[b]
					143 − 290; 148[c]	1 − 142, 291 − 366; 218[c]
2013	36 − 137; 102	138 − 224; 87	225 − 334; 110	1 − 35, 335 − 365; 66	139 − 287; 149[a]	1 − 138, 288 − 365; 216[a]
					121 − 304; 184[b]	1 − 120, 305 − 365; 181[b]
					127 − 297; 171[c]	1 − 126, 298 − 365; 194[c]
2014	49 − 127; 79	128 − 228; 101	229 − 309; 81	1 − 48, 310 − 365; 104	137 − 288; 152[a]	1 − 136, 289 − 365; 213[a]
					121 − 304; 184[b]	1 − 120, 305 − 365; 181[b]
					142 − 294; 153[c]	1 − 141, 295 − 365; 212[c]
2015	36 − 150; 115	151 − 224; 74	225 − 312; 88	1 − 35, 313 − 365; 88	145 − 288; 144[a]	1 − 144, 289 − 365; 221[a]
					121 − 304; 184[b]	1 − 120, 305 − 365; 181[b]
					136 − 295; 160[c]	1 − 135, 296 − 365; 205[c]
2016	47 − 161; 115	162 − 225; 64	226 − 299; 74	1 − 46, 300 − 366; 113	141 − 287; 147[a]	1 − 140, 288 − 366; 219[a]
					122 − 305; 183[b]	1 − 120, 305 − 366; 182[b]
					140 − 296; 157[c]	1 − 139, 297 − 366; 209[c]

39

813   **Note:** [a], based on vegetation cover and temperature change (VCT) (Lund et al., 2010; Tang and Arnone, 2013; Song et al., 2015); [b], based on Julian

814   months (JMC) (Da et al., 2015); [c], based on vegetation phenology change (VPC). Spring , Summer, Autumn, Winter are based on parameters of

815   microbial activities, ALT variety coefficient and T_{soil} (SMT).

816

817

818

819

820

821

822

823

824

825

826

827

828   **Table 3.** Correlation coefficients between CH_4 fluxes and environment factors on half–hour time scales

| Environment | CH₄ Flux | | | | | | | | | |
| | Spring | | Summer | | Autumn | | Winter | | 2012 − 2016 | |
Factors	r	n	r	n	r	n	r	n	r	n
T_{air}	0.25**	24144	0.14**	19818	-0.16**	20959	0.32**	22224	-0.11**	87145
Wind Speed	0.31**	24144	-0.04**	19817	-0.20**	20959	0.32**	22224	0.15**	87144
VPD	-0.33**	18624	-0.21**	19263	-0.09**	16737	-0.21	18000	0.26**	69624
Rn	0.55**	24143	0.09**	19807	-0.33**	20913	0.51**	22224	0.09**	87087
Albedo	0.07**	24144	-0.01	19814	-0.08**	20913	0.10**	22224	0.02**	87095
SHF of 5cm	0.46**	24144	-0.08**	19818	-0.23**	20913	0.43**	22224	0.09**	87099
SHF of 15cm	0.36**	24144	-0.15**	19815	-0.23**	20913	0.33**	22224	0.08**	87096
SWC of 10cm	-0.16**	24144	-0.14**	19818	-0.06**	20959	0.00	22224	-0.25**	87145
SWC of 20cm	-0.15**	24144	-0.13**	19816	-0.07**	20959	0.11**	22224	-0.24**	87143
SWC of 40cm	-0.11**	24144	-0.02**	19818	0.07**	20959	0.06**	22224	-0.17**	87145
SWC of 80cm			-0.13**	19818	0.06**	20959				
SWC of 160cm			0.04**	19818	-0.11**	20959				
Precipitation			-0.02	16748	0.01[b]	17888				
ALT	0.73**	23004	0.23**	19823	0.73**	21454			0.43**	64281

ΔI	0.77**	100	0.57**	83	0.46**	89	0.23	93	0.49**	365
ΔII	0.31**	100	0.66**	83	0.78**	89	0.19	93	0.52**	365
T_{soil} of 0 cm	-0.06*	23004	0.13**	19823	0.07**	20366	0.13**	21711	0.11**	84904
T_{soil} of 5 cm	0.15**	24144	0.15**	19808	-0.13**	21454	0.27**	22224	0.24**	87630
T_{soil} of 10 cm	-0.03**	24144	0.12**	19808	0.08**	21454	0.16**	22224	0.13**	87630
T_{soil} of 20 cm	-0.14**	24144	0.08**	19808	0.02**	21454	0.06**	22224	-0.09**	87630
T_{soil} of 30 cm	-0.13**	23004	0.06**	19823	-0.02**	20366	0.07**	21711	-0.08**	84904
T_{soil} of 40 cm	0.14**	24144	0.05**	19808	-0.01[b]	21454	0.06**	22224	0.11**	87630
T_{soil} of 50 cm			0.04**	19823	-0.05**	20366				
T_{soil} of 70 cm			0.07**	19823	-0.05**	20366				
T_{soil} of 80 cm			0.05**	19808	0.04**	21454				
T_{soil} of 100 cm			0.10**	19823	-0.05**	21454				
T_{soil} of 150 cm			0.09**	19823	-0.04**	20366				
T_{soil} of 160 cm			0.10**	19808	0.01**	21454				
T_{soil} of 200 cm			0.02**	19823	-0.02**	20366				

829 **Note:** ** means $p<0.01$, * means $p<0.05$; r values for the relationship between CH_4 flux and environment factors. T_{air} means air temperature of 3 m

830 above the ground surface. VPD is vapor pressure deficit, NR is net radiation, and SWC is soil water content, ALT is active layer thickness, which fitted

831 through the depth of soil 0 °C in Surfer 8.0., and the data is removed as meaningless in winter. T_{soil} is the temperature of the soil. In spring and winter,

832   precipitation data is too sparse for statistical analysis. ΔI is the soil $0 - 25cm$ archaeal methanogens gene expression, and ΔII is the soil $0 - 25\ cm$

833   methanotrophic gene expression. The coefficients (r) between CH_4 flux and ΔI, ΔII are obtained using the synchronous CH_4 fluxes averaged for 5 days.

834

835

836

837

838

839

840

841

842

843

844

845   **Table 4**. Principal components analysis (PCA) of the environmental factors.

Component	Spring				Summer				Autumn				Winter			
	PC1	PC2	PC3	PC4	PC1	PC2	PC3	PC4	PC1	PC2	PC3	PC4	PC1	PC2	PC3	PC4
wind speed	-0.03	0.51	0.65	-0.46	0.02	0.37	0.38	-0.13	-0.04	0.44	0.59	0.67	0.27	0.45	-0.11	-0.27
T_{air}	0.38	0.29	-0.05	-0.11	0.42	0.22	-0.03	0.02	0.36	0.21	0.08	-0.06	0.48	0.12	-0.02	0.01
VPD	0.34	-0.27	0.40	0.15	0.17	0.46	-0.22	0.09	0.34	-0.15	0.17	-0.07	0.14	-0.15	0.95	-0.22
Rn	0.16	0.49	0.00	0.76	-0.01	0.07	0.58	0.11	0.12	0.54	-0.43	-0.07	0.26	0.47	-0.01	-0.49
SHF of 15cm	0.24	0.49	-0.30	-0.09	0.25	0.53	-0.09	0.01	0.15	0.59	-0.23	-0.15	0.36	0.37	0.14	0.58
ALT	0.22	-0.40	0.40	0.27	0.32	-0.53	-0.05	0.02	0.29	0.49	0.70	0.25				
ΔI	0.49	-0.22	0.01	-0.08	0.50	-0.16	0.02	-0.16	0.29	0.31	0.24	-0.51	0.52	0.05	0.07	-0.03
SWC of 10 − 20cm													-0.31	0.45	0.22	0.47
SWC of 10 − 40cm	0.33	-0.20	0.50	0.25	-0.16	0.15	-0.16	0.73	0.28	-0.18	-0.41	0.53				
SWC of 50 − 160cm					0.23	-0.20	-0.16	0.55	0.31	-0.17	-0.32	0.41				
Precipitation					0.03	-0.04	0.63	0.35								
T_{soil} of 0 cm	0.43	-0.07	-0.20	-0.27	0.43	0.08	0.08	-0.07	0.37	0.07	0.19	-0.16	0.43	-0.35	-0.15	0.09
T_{soil} of 5 − 20 cm	0.44	-0.01	-0.17	-0.16									0.45	-0.28	0.00	0.28
T_{soil} of 5 − 40 cm					0.46	-0.05	0.04	-0.03	0.38	0.02	0.18	-0.17				
T_{soil} of 30 − 50cm	0.40	-0.23	-0.08	-0.04												
T_{soil} of 50 − 80cm					0.37	-0.36	0.00	0.01	0.37	-0.11	0.19	-0.14				
T_{soil} of 100 − 200cm					0.33	-0.34	0.01	-0.01	0.36	-0.14	0.08	0.00				
Percent of variance	0.63	0.23	0.08	0.04	0.70	0.18	0.07	0.02	0.69	0.17	0.08	0.04	0.75	0.21	0.02	0.01
Cumulative	0.63	0.86	0.94	0.98	0.70	0.88	0.95	0.97	0.69	0.86	0.94	0.98	0.75	0.96	0.98	0.99

846   **Note:** PC means principal component. Before PCA, SWC was divided for three parts, 10 – 20 cm, 10 – 40 cm, and 50 – 160 cm according to collinearity

847   test in four seasons. T_{soil} was divided for six parts of T_{soil} of 0 cm, T_{soil} of 5 – 20 cm, T_{soil} of 5 – 40 cm, T_{soil} of 30 – 50 cm, T_{soil} of 50 – 80 cm, and T_{soil}

848   of 60 – 200 cm according to collinearity test in different seasons.

849

850
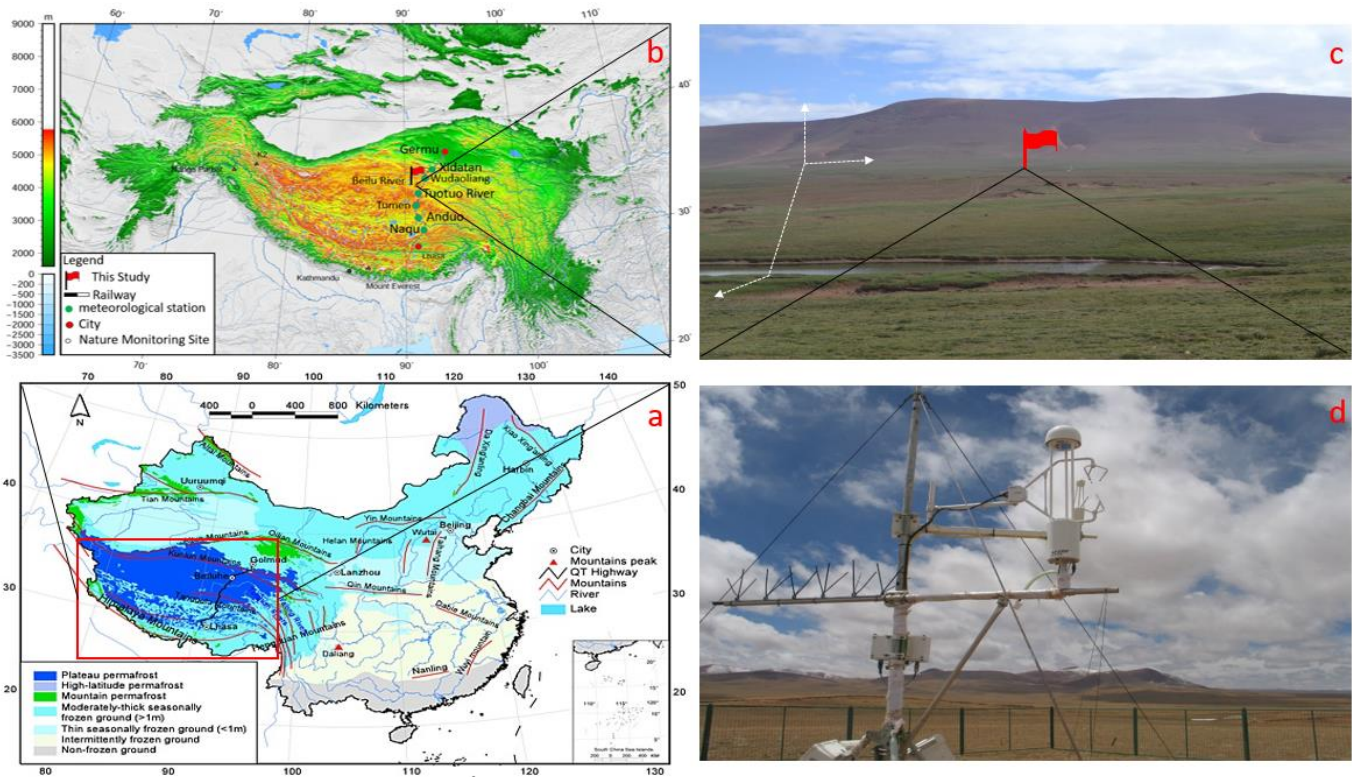
Figure 1. Geographic location of the study site: (a) is a map of China's permafrost distribution, and the red box marks the approximate location of the Qinghai–Tibet Plateau; (b) shows the study site location and meteorological stations along the Qinghai–Tibet railway; (c) is the photo showing the study site's topography and physiognomic. The small red flag in (c) is the eddy covariance tower location; (d) is the close–up shot of the LI–7700 for methane measurement. *Map boundary and location are approximate. Geographic features and the names do not imply any official endorsement or recognition*

857

858
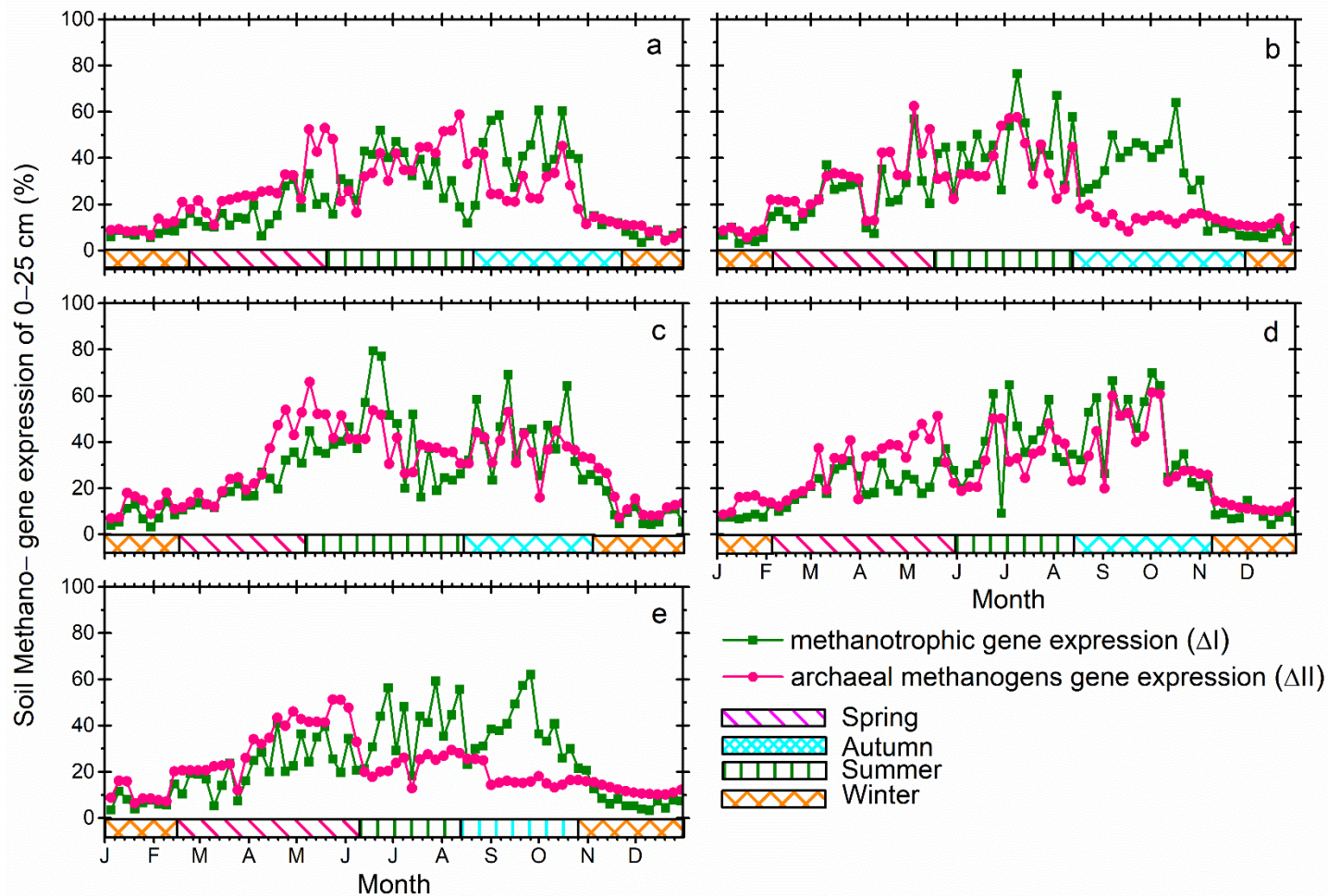
Figure 2. Annual patterns of soil methanogen−gene expression of 0 − 25 cm soil depth for years: (a) 2012, (b) 2013, (c) 2014, (d) 2015, and (e) 2016.
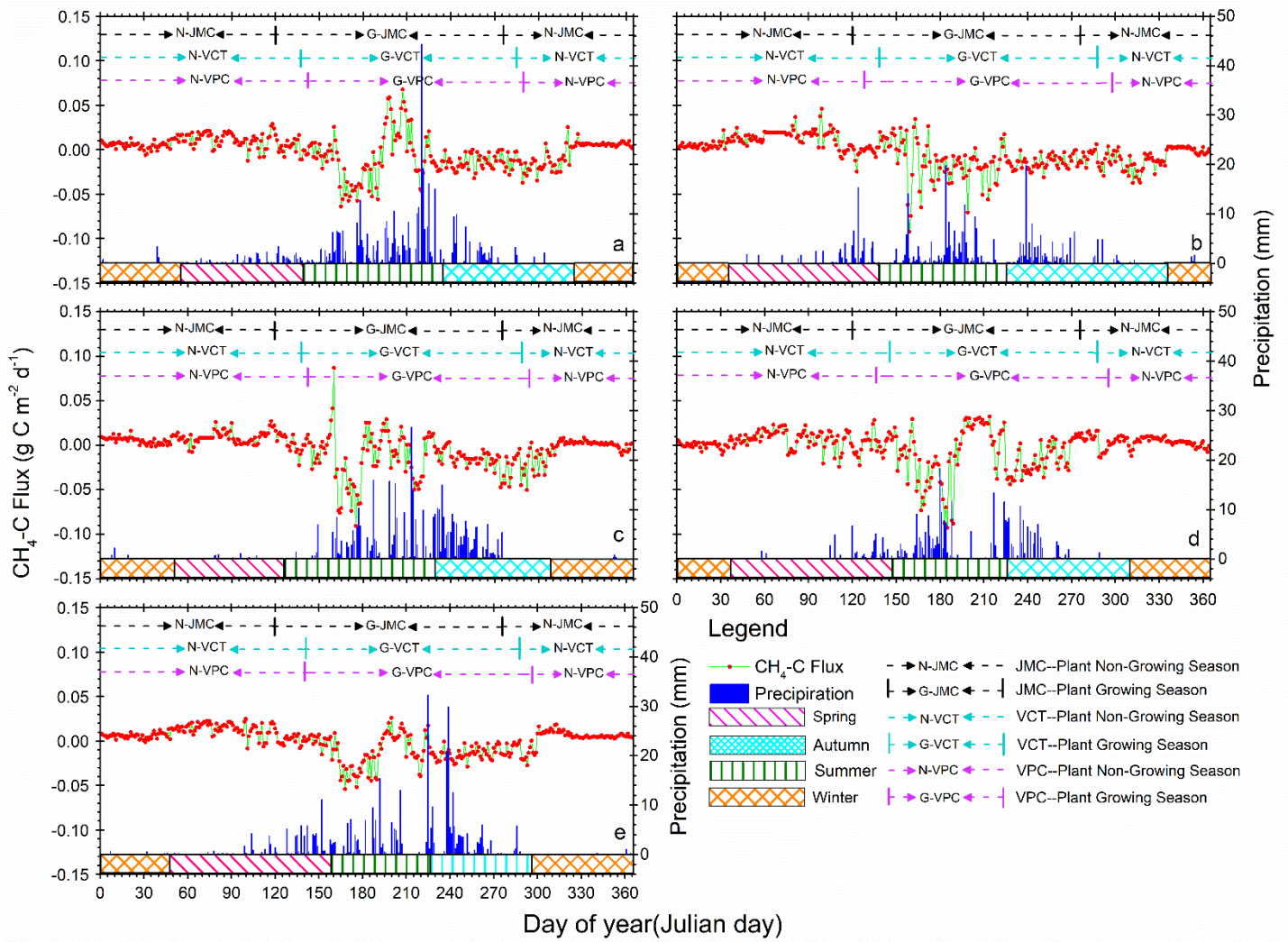
Figure 3. Annual patterns of diel methane (CH_4) flux and precipitation variations from 2012 to 2016. Positive values indicate CH_4 release and negative values indicate CH_4 uptake by ecosystems. Red dots and light green lines are CH_4–C flux variation, and the deep blue histograms show diel precipitation accumulation. Pink, olive, cyan, and orange blocks mean spring, summer, autumn, and winter seasons respectively, according to our new method of SMT (see Methods). Black, cyan, and pink dotted lines with bars separated the plant growing from non–growing seasons and stand for seasons by the method JMC, VCT, and VPC, respectively. Details about the methods JMC, VCT, and VPC can be found in section 3.2.

878
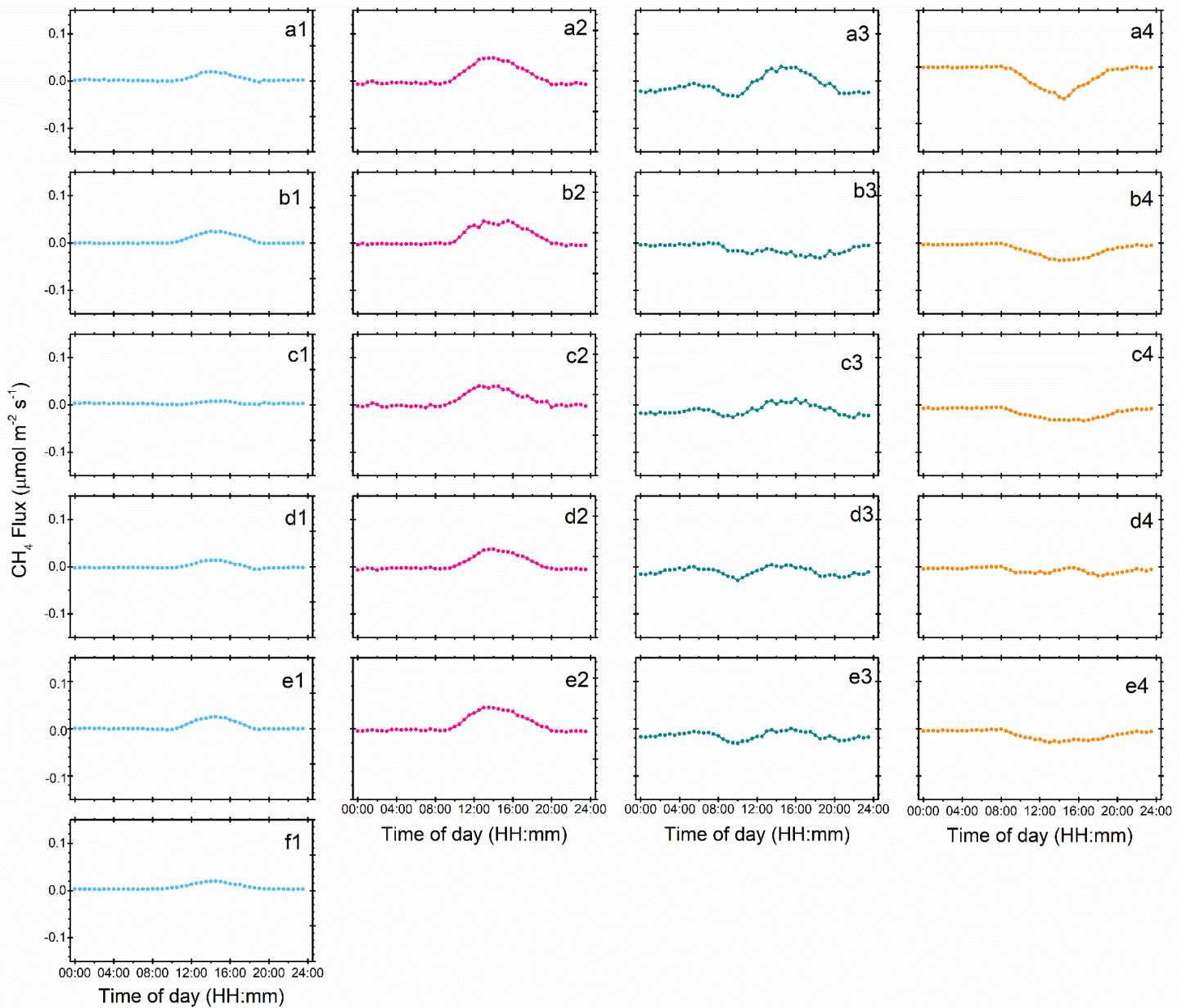
Figure 4. Diel CH$_4$ fluxes from 2012 to 2016 for different seasons. Blue, pink, green and orange, represent

winter, spring, summer, and autumn, respectively; (a1), (a2), (a3), and (a4) are for 2012; (b1), (b2), (b3), and

(b4) are for 2013; (c1), (c2), (c3) and (c4) are for 2014; (d1), (d2), (d3), and (d4) are for 2015; (e1), (e2), (e3),

(e4) and (f1) are for 2016.
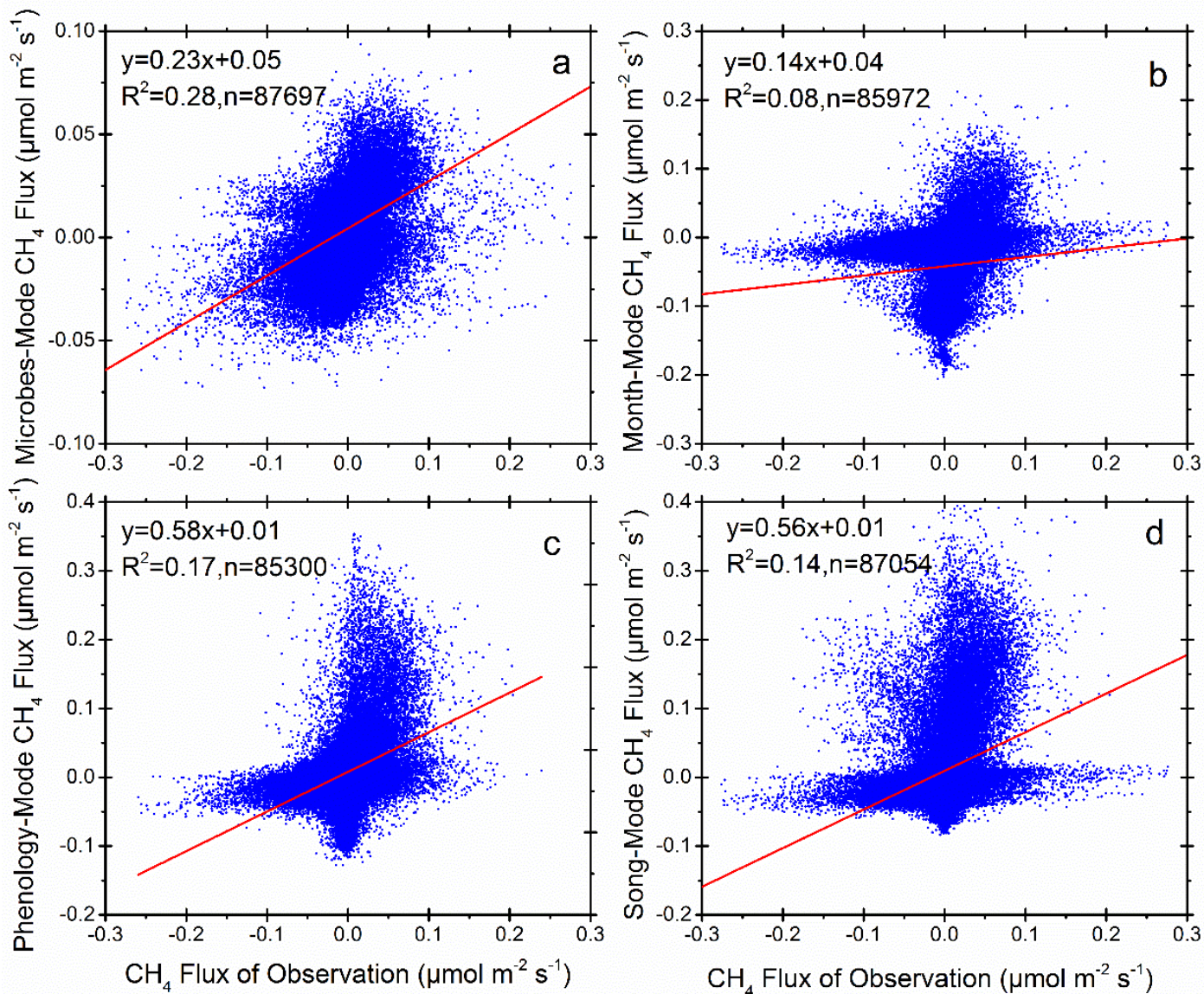
883

884 **Figure 5.** Regression comparison between observation and modeled methane fluxes with four different seasonal

885 definitions and classification models. Panels (a), (b), (c), and (d) are for the SMT, JMC, VCT, and VPC

886 methods, respectively.

887

888

889

890
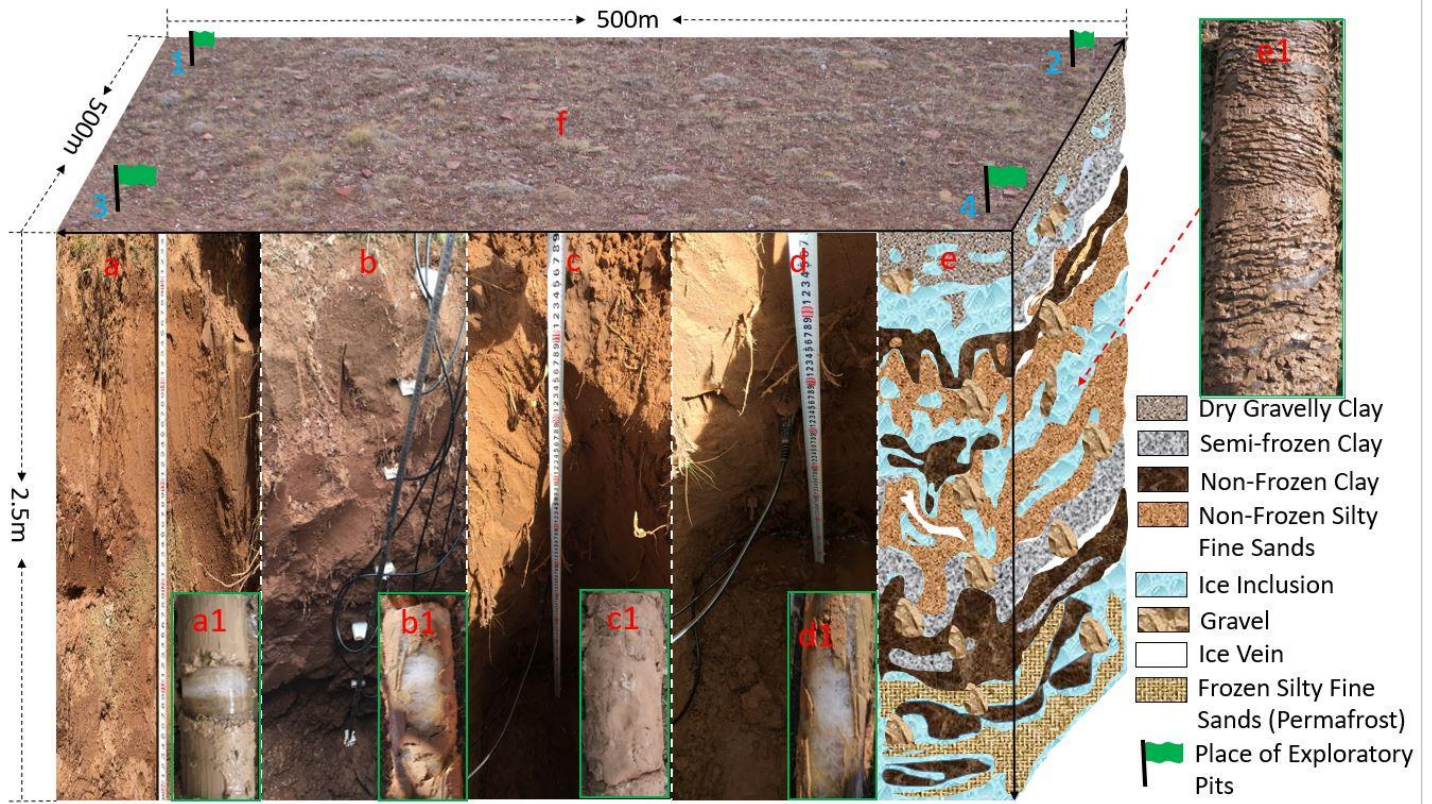
Figure 6. Location of exploratory pits and drillings in this study in autumn: (f) is photo of a typical ground surface (October 16th, 2014). Green flags represent the location for the soil survey by test pits and drilling. (a), (b), (c), and (d) show soil profiles of 0 − 250 cm depths at the North (1), South (2), East (3), and West (4) corners of the eddy covariance footprint, respectively. (a1), (b1), (c1), and (d1) are drilling cores, with clear ice (white) in (a1), (b1), and (d1), but not in (c1); (e) provides an illustration that combines results from drillings, test pits and multi–channel ground–penetrating radar (Malå Geoscience, Sweden) for active layer variations in permafrost area during the autumn season; and (e1) is a core sample of the same drilling (October 16th, 2014).

Supplement

Supplementary Table 1 Seasonal soil water content (SWC, %) of winter, spring, summer, and autumn from 2012

to 2016.

Seasonal	Period	10 cm	20 cm	40 cm	80cm	160cm
		Soil Water Content (SWC), %				
Winter	2012 early	0.11	0.08	0.07	0.11	0.14
	2012-2013	0.10	0.08	0.07	0.11	0.16
	2013-2014	0.10	0.08	0.07	0.11	0.13
	2014-2015	0.10	0.08	0.07	0.11	0.17
	2015-2016	0.10	0.08	0.07	0.11	0.16
	2016 later	0.10	0.08	0.07	0.12	0.19
	Average	0.10	0.08	0.07	0.11	0.16
Spring	2012	0.13	0.09	0.08	0.11	0.13
	2013	0.12	0.09	0.08	0.11	0.13
	2014	0.12	0.08	0.07	0.11	0.13
	2015	0.13	0.09	0.08	0.11	0.14
	2016	0.12	0.09	0.08	0.13	0.15
	Average	0.12	0.08	0.08	0.11	0.14
Summer	2012	0.18	0.11	0.10	0.17	0.27
	2013	0.16	0.11	0.11	0.19	0.25
	2014	0.16	0.10	0.10	0.16	0.24
	2015	0.16	0.10	0.10	0.19	0.28
	2016	0.16	0.10	0.09	0.18	0.28
	Average	0.17	0.10	0.10	0.18	0.26
Autumn	2012	0.14	0.09	0.08	0.14	0.21
	2013	0.14	0.09	0.09	0.15	0.20
	2014	0.16	0.10	0.10	0.16	0.22
	2015	0.15	0.10	0.09	0.15	0.21
	2016	0.16	0.10	0.09	0.16	0.21
	Average	0.15	0.10	0.09	0.15	0.21

908
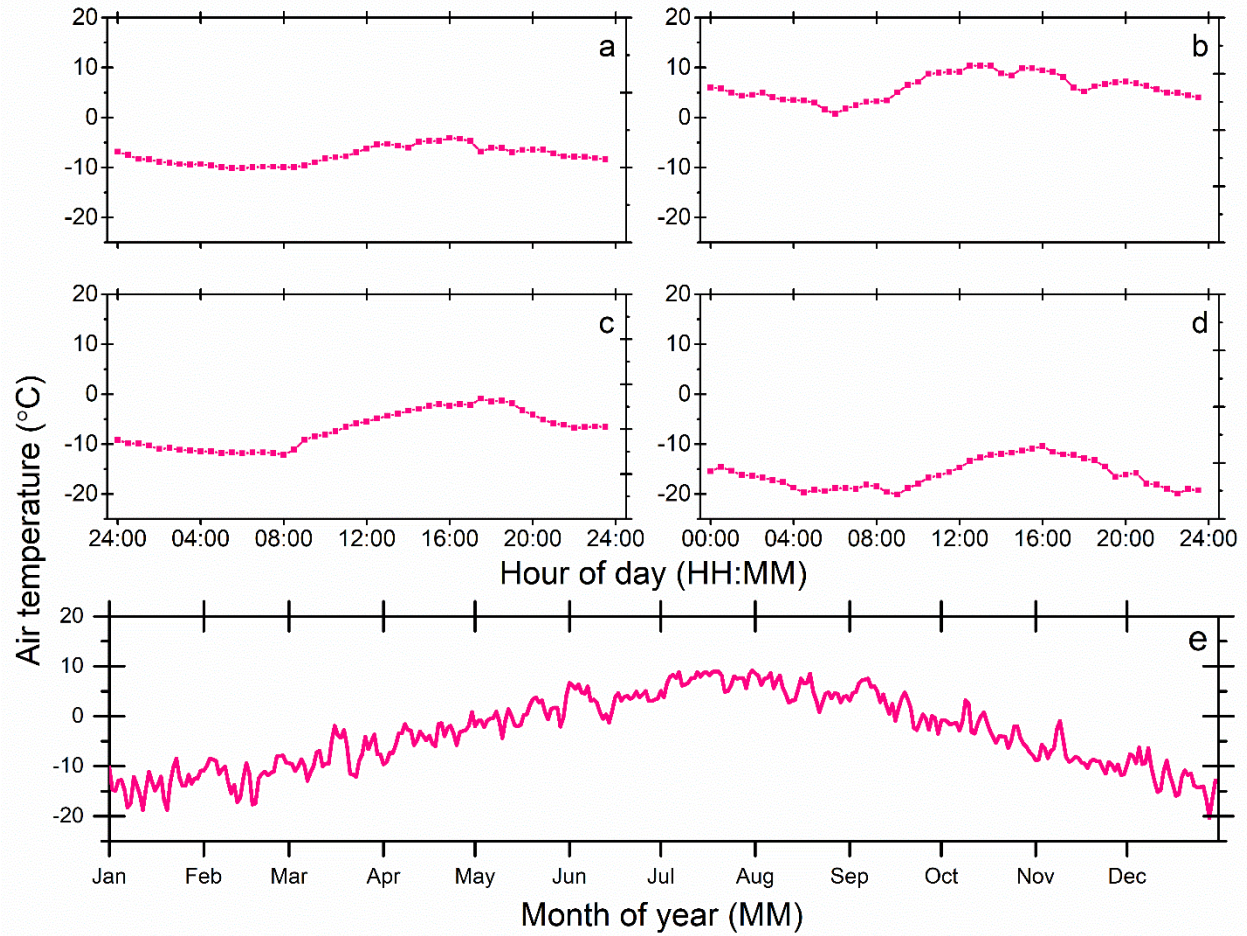
Supplementary Figure 1. Air temperature (T_{air}) measured 3 meters above the ground surface:
(a), (b), (c), and (d) are half–hourly mean values in spring, summer, autumn, and winter,
respectively; (e) shows diel–scale mean values from 2012 to 2016.

912
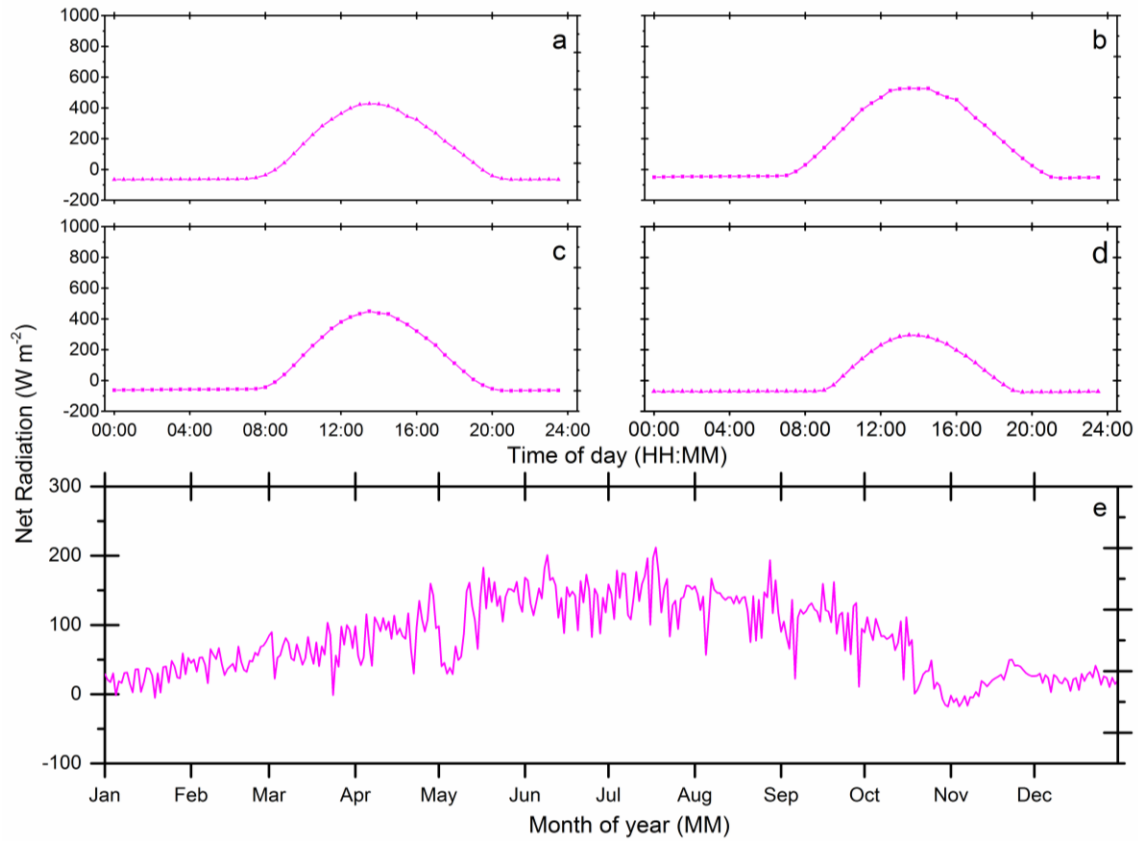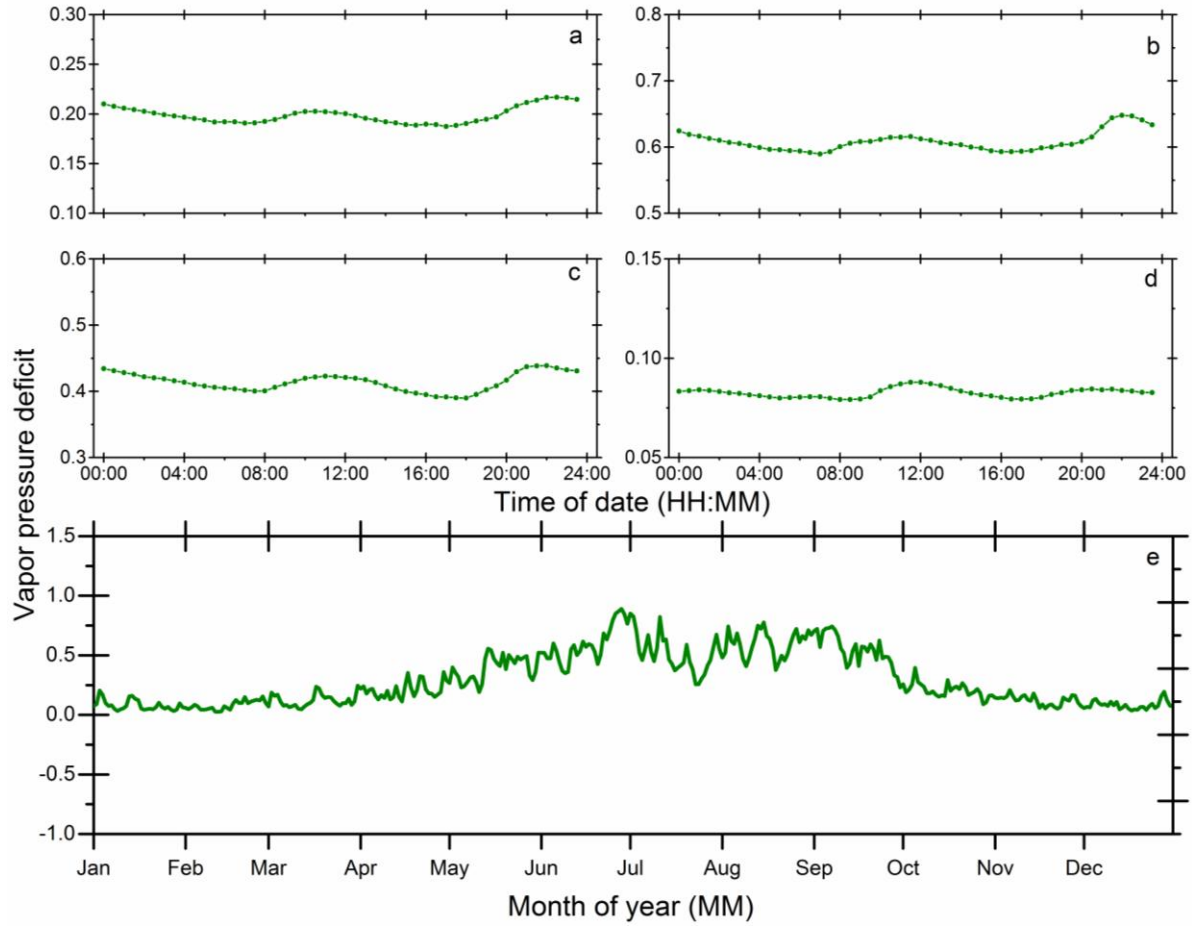
Supplementary Figure 2. Net radiation (Rn) measured 3 meters above the ground surface: (a),

(b), (c), and (d) are half–hourly mean values in spring, summer, autumn, and winter,

respectively; (e) shows diel–scale mean values from 2012 to 2016.

916

Supplementary Figure 3. Vapor pressure deficit (VPD) measured 3 meters above the ground surface: (a), (b), (c), and (d) are half–hourly mean values in spring, summer, autumn, and winter, respectively; (e) shows diel mean values from 2012 to 2016.

Legend:
- 0 - 4 meter
- 4 - 8 meter
- 8 - 12 meter
- >= 12 meter

924
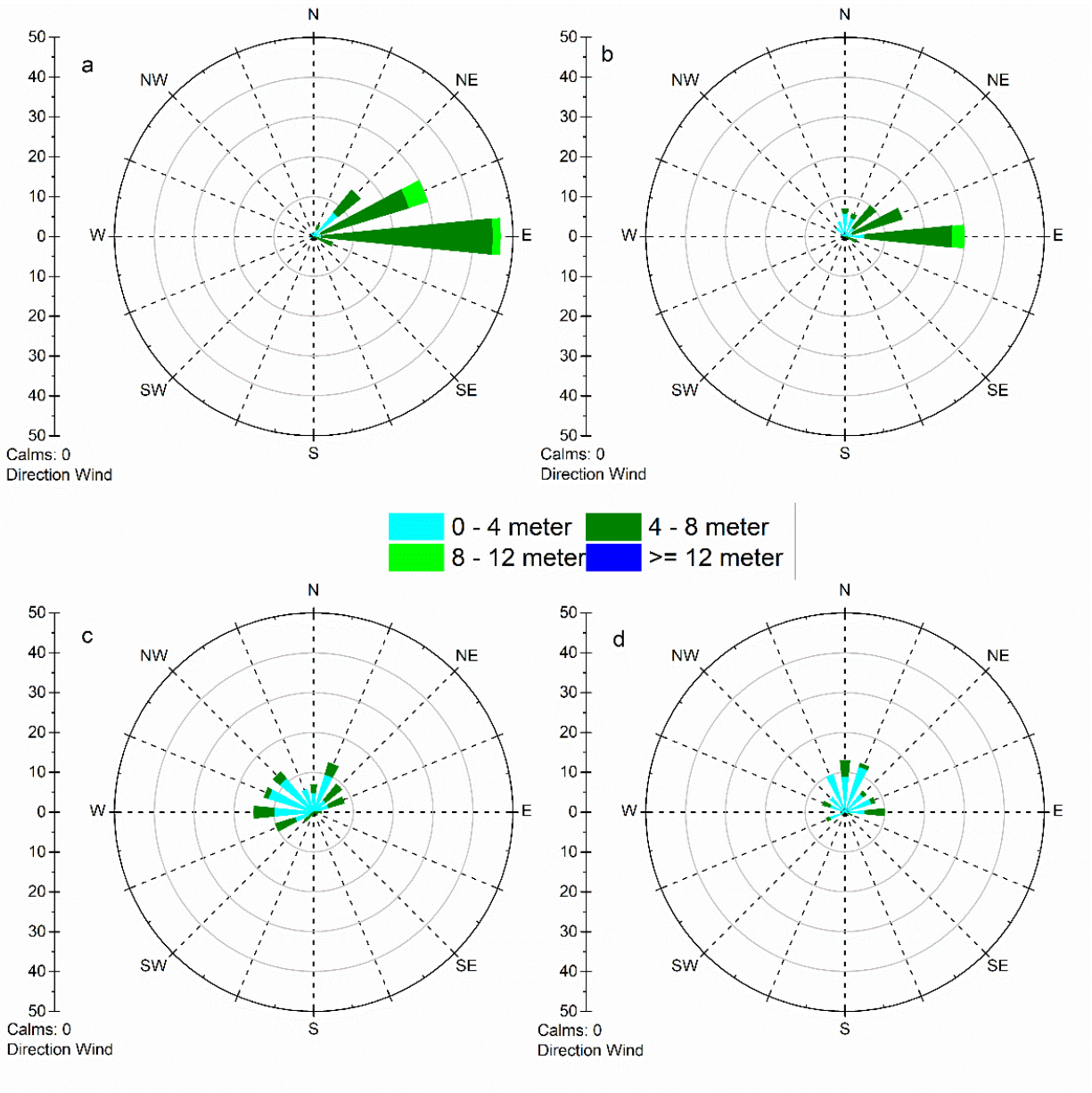
Supplementary Figure 4. Diel mean of wind speed and direction between 2012 and 2016: (a) is
winter, (b) is spring, (c) is summer, and (d) is autumn. Note the direction of wind means the
direction wind blows *from*. All data are presented as mean values with standard deviations (mean
± standard deviation).

929

930

931

932
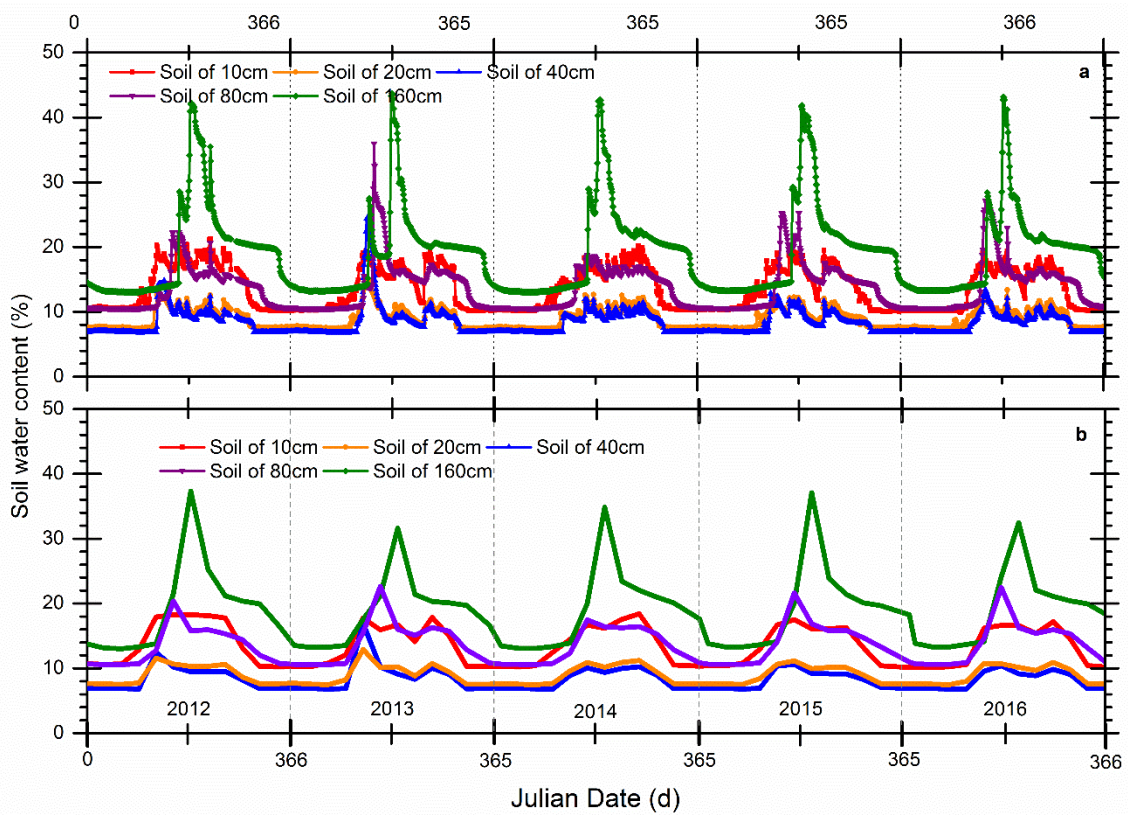
Supplementary Figure 5. Comparison between soil water content (SWC) of two different time

resolutions from 2012 to 2016, (a) is the half–hourly SWC at soil depths of 10 cm, 20 cm, 40 cm,

80 cm, and 160 cm; and (b) is the 4–hourly mean SWC for the same depths.

936
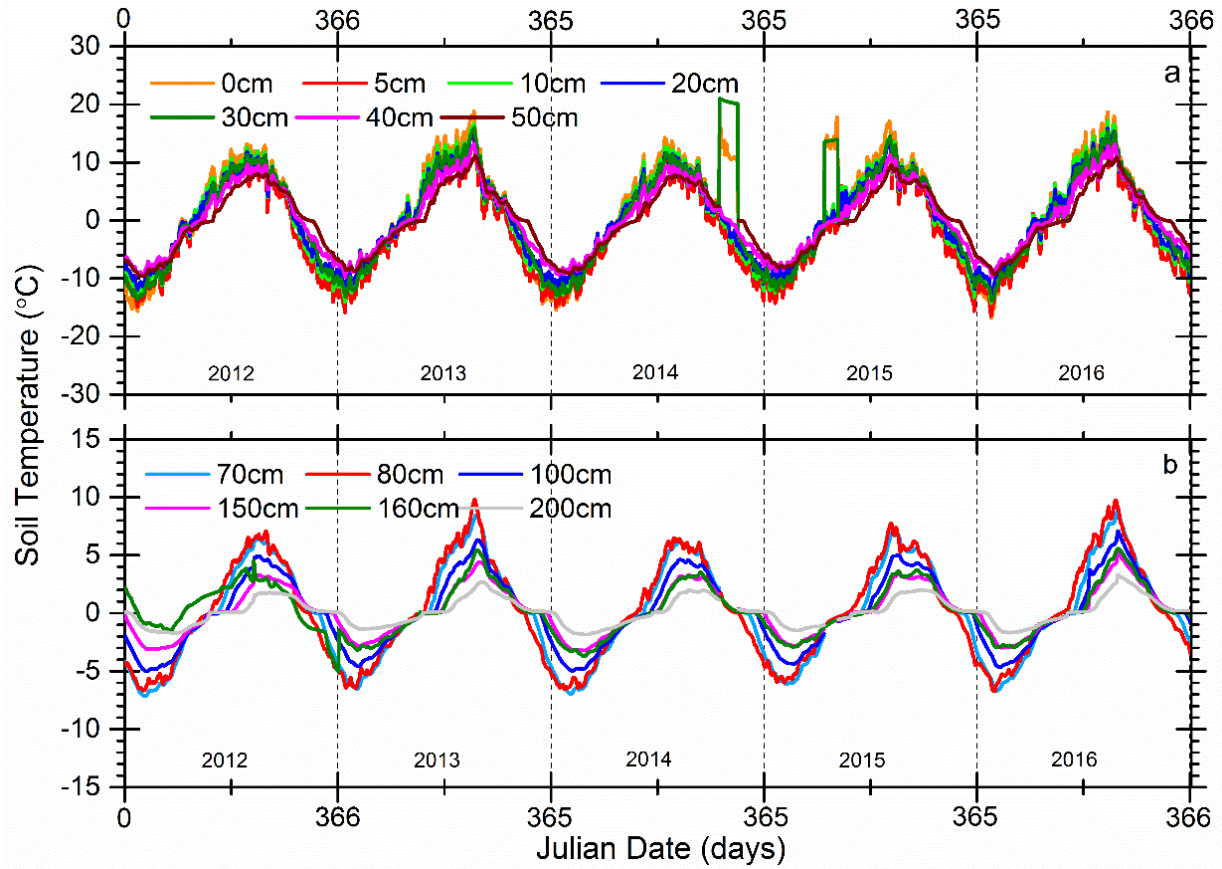
Supplementary Figure 6. Half–hour measurements of $0 - 200$ cm soil temperature (T_{soil}) variations from 2012 to 2016, (a) is for soil depths of 0 cm, 5 cm, 10 cm, 20 cm, 30 cm, 40 cm, 50 cm, (b) is for soil depth of 70 cm, 80 cm, 100 cm, 150 cm, 160 cm, and 200 cm.
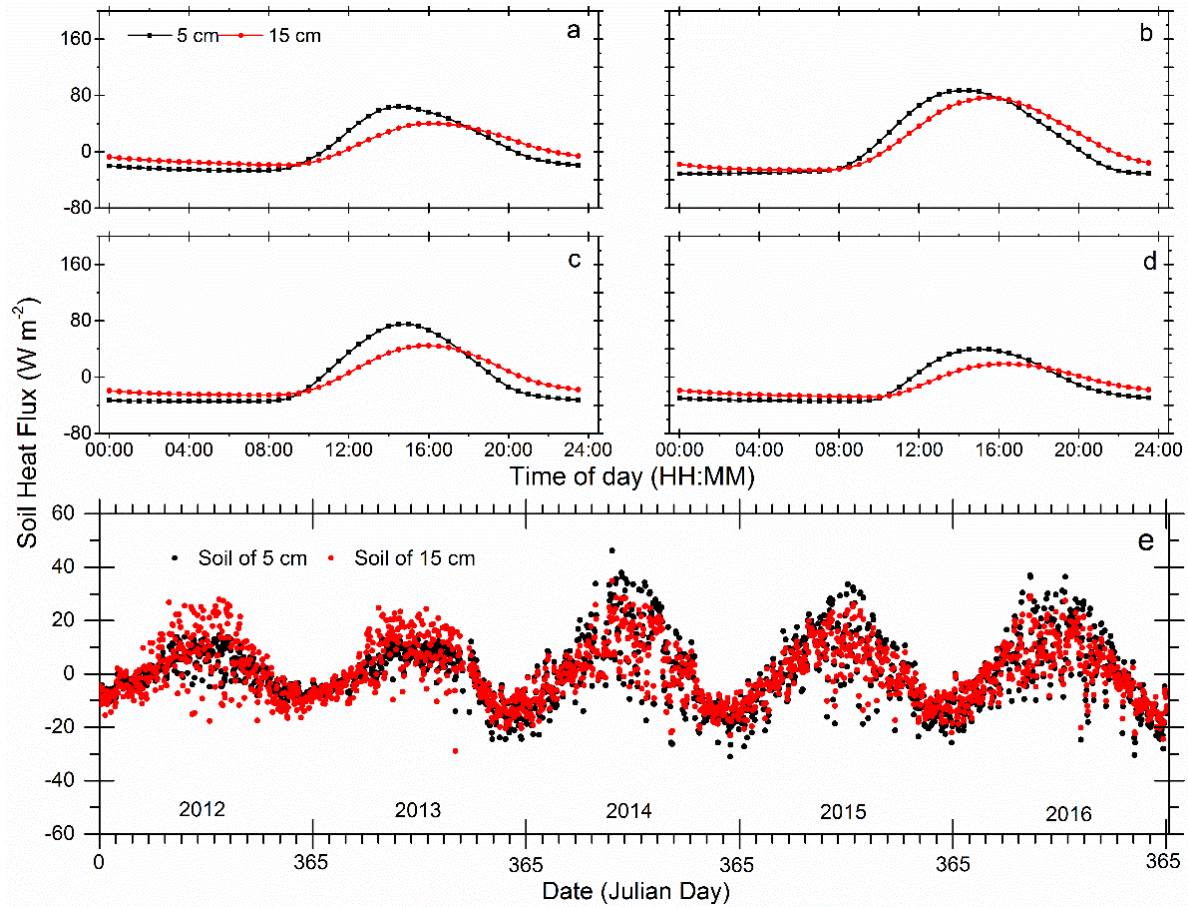
Supplementary Figure 7. Soil heat flux (SHF) at depth of 5 cm and 15 cm: (a), (b), (c), and (d) are half–hourly mean values in spring, summer, autumn, and winter, respectively; (e) shows diel mean values from 2012 to 2016.
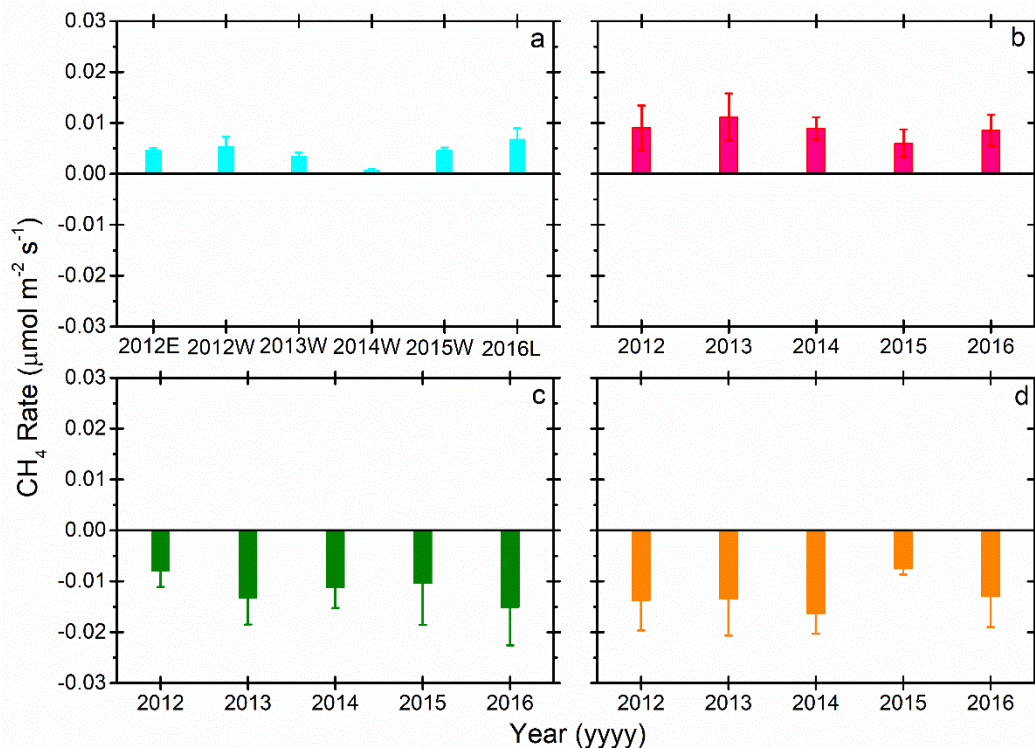
.
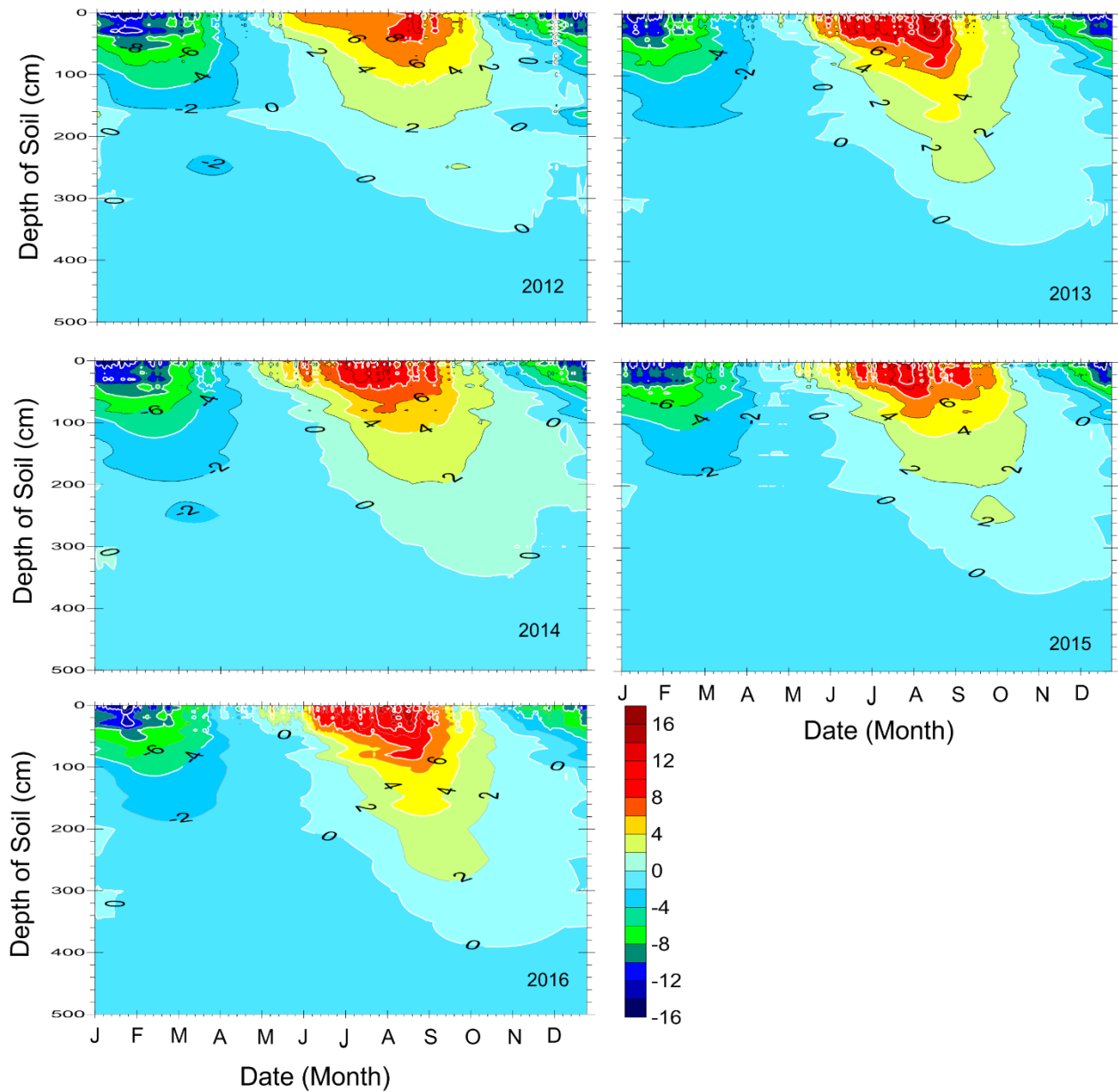
Supplementary Figure 8. Characteristics of the seasonal freezing and thawing processes of the active layer for years: 2012, 2013, 2014, 2015, and 2016. Different colors represent the soil temperature gradients from -16 °C to 20 °C. The depth of 0 °C represent the active layer thickness (ALT).

952

Supplementary Figure 9. Seasonal CH_4 rate mean value from 2012 to 2016: (a) is winter, (b) is spring, (c) is summer, and (d) is autumn. In the (a), 2012E is started from January 1st, 2012 and ended on February 17th, 2012; 2012W is started from 19th November, 2012 to 4th February, 2013; 2013W is started from 1st December, 2013 to 17th February, 2014; 2014W is started from 6th November, 2014 to 4th February, 2015; 2015W is started from 9th November, 2015 to 15th February, 2016; 2016L is started from October 26th, 2016 and ended on December 31st, 2016. All data are presented as mean values with standard deviations (mean ± standard deviation).

960
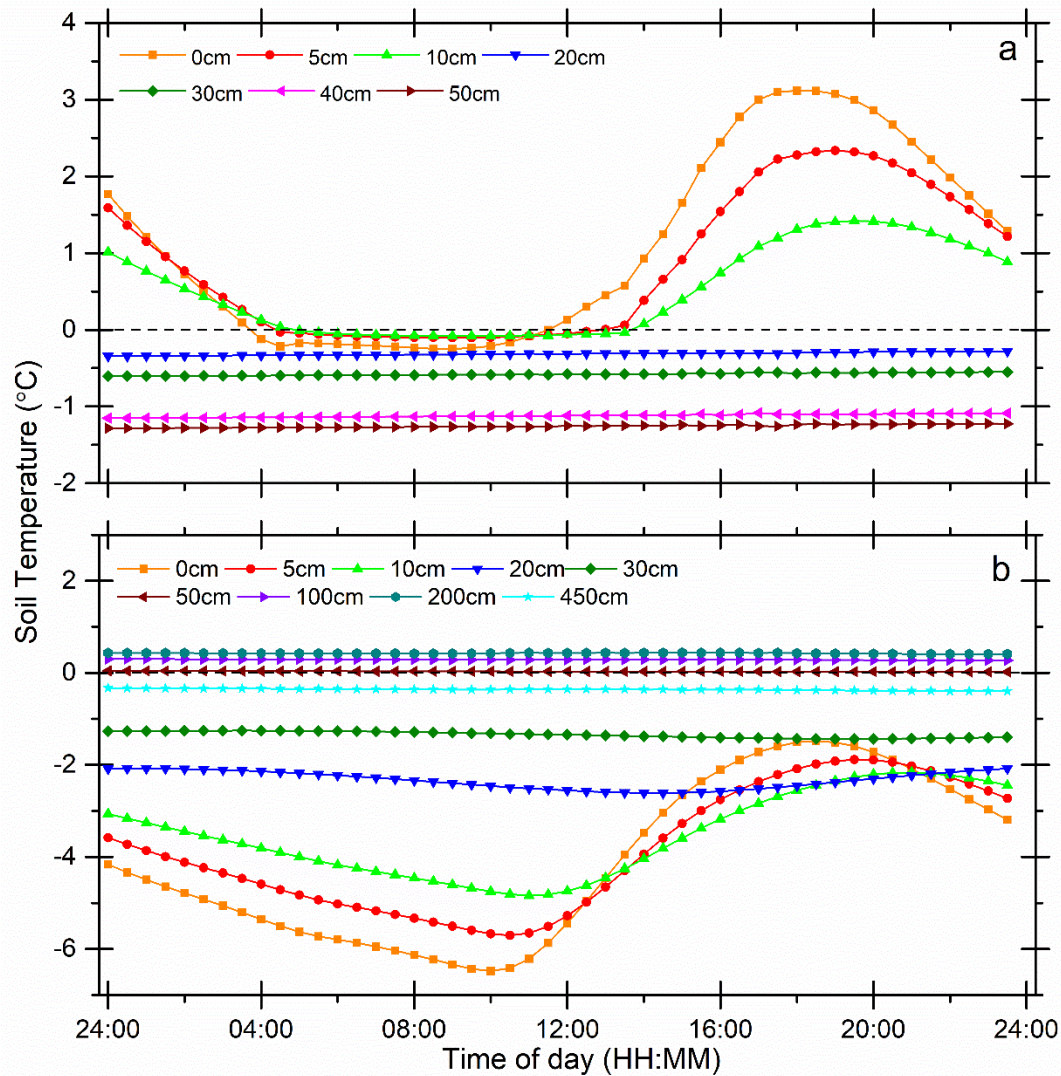
Supplementary Figure 10. Mean half–hourly values of $0 - 450$ cm soil temperature (T_{soil}) from

2012 to 2016, (a) is for spring, (b) is for autumn. Note, that during spring T_{soil} of 100cm, 200cm,

450cm is always below -2 °C and during autumn the T_{soil} of 40cm almost overlap to T_{soil} with

50cm. To make the figure more readable, we removed the T_{soil} values of 100cm, 200cm, 450cm

in figure (a) and removed the T_{soil} values of 40cm for figure (b).
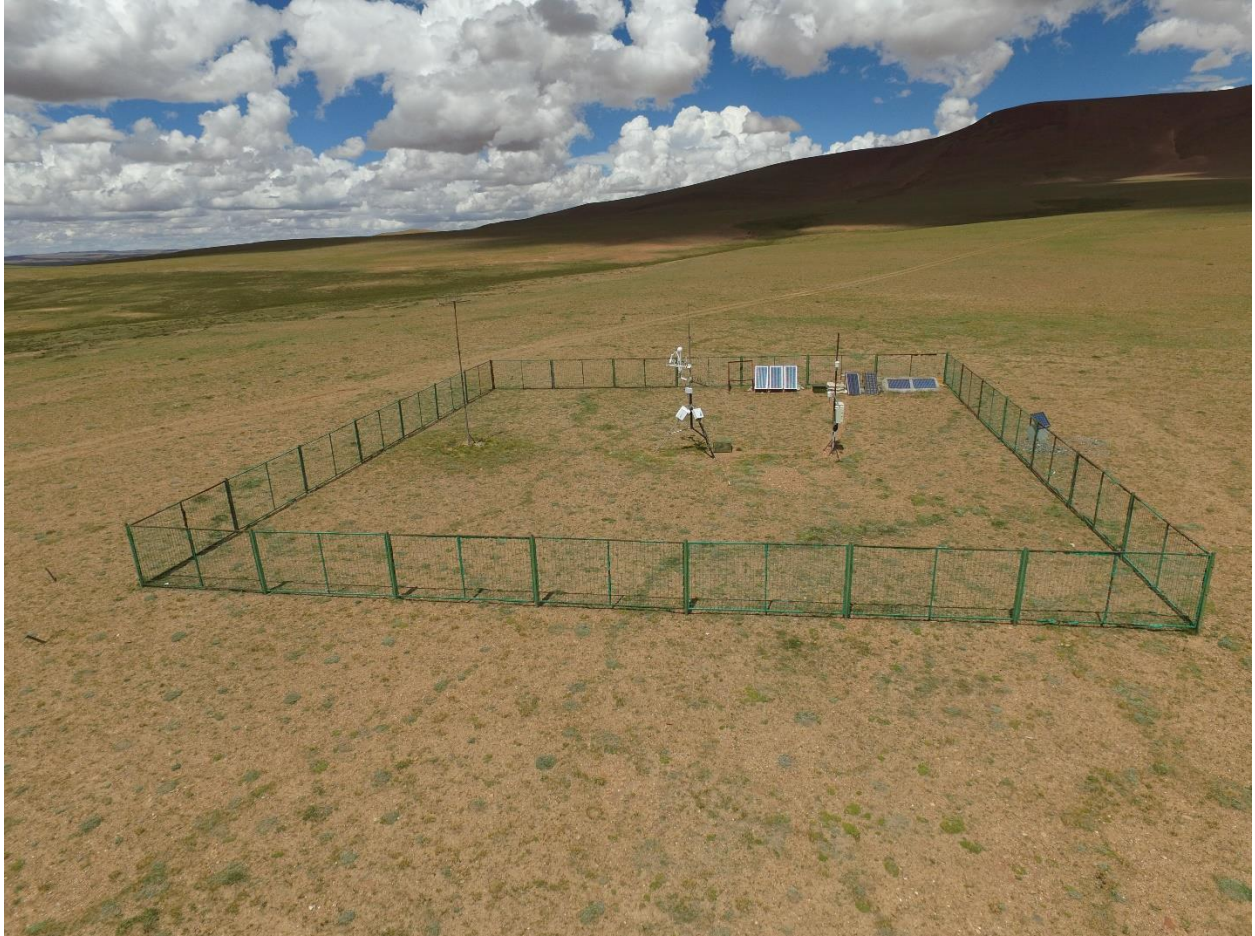
966

967   **Supplementary Figure** 11. A bird's eye view of the eddy covariance site at the Beilu'he station